Check for updates

Anti-filarial efficacy of *Centratherum anthelminticum*: unravelling the underlying mechanisms through biochemical, HRAMS proteomics and MD simulation approaches†

Sunil Kumar, Ayushi Mishra, Surya Pratap Singh ![ORCID] and Anchal Singh ![ORCID] *

Traditionally, *Centratherum anthelminticum* (CA) has been reported to be a potent anti-filarial, however no reports are available detailing its mechanism of action against filarial parasites. In this study, we have evaluated the anti-filarial activity of CA against lymphatic filarial parasites *Setaria cervi* using *ex vivo* biochemical, proteomics and *in silico* approaches. The motility and viability of the parasites decreased significantly after treatment with CA concentrations of $\geq$125 µg mL^{-1}. An increase in lipid peroxidation (51.92%), protein carbonylation (48.99%), NADPH oxidase (88.88%) activity and decrease in the glutathione (GSH) (−39.23%), glutathione reductase (GR) (−60.17%), and glutathione S-transferase (GST) (−50.48%) activity was also observed after CA treatment. The proteomics analysis was performed by two-dimensional gel electrophoresis and high-resolution accurate mass spectrometry (HRAMS). In total, 185 proteins were differentially expressed (DEPs) following CA treatment. The major DEPs were mostly involved in tRNA processing, biosynthetic processes, metabolic activities, protein transport, the tricarboxylic acid cycle, protein translation, and stress response. The UPLC-ESI-MS/MS analysis of CA extract revealed the presence of 40 bioactive compounds. Further the docking analysis showed 10 CA bioactive compounds to have high binding affinity towards antioxidant proteins of filarial parasites. Additionally, MD simulation studies showed stable interactions (RMSF $\leq$ 10 Å) of 3-*O*-methylquercitin, quinic acid, gentisic acid, and vanillin with filarial antioxidant enzymes/proteins. To our knowledge, this is the first report detailing the molecular mechanism of anti-filarial activity of CA, which can be further evaluated for the development of new anti-filarial formulations.

1 Introduction

Lymphatic filariasis (LF) is a serious health problem caused by nematode parasites *Wuchereria bancrofti*, *Brugia malayi*, and *Brugia timori*. LF is prevalent in large parts of the tropical and subtropical regions of the world and more than 50 million people in 44 countries are infected while another 882 million people are at the risk of infection (**https://www.who.int/news-room/fact-sheets/detail/lymphatic-filariasis**). The World Health Organization aims to globally eradicate LF, through the implementation of a Mass Drug Administration (MDA) plan. This strategy entails providing pairs of anthelminthic medications (Albendazole with either Ivermectin or Diethylcarbamazine) to the entire population at risk.[1] These drugs can reduce the microfilaria reservoir but cannot kill adult worms.[2] Administration of Diethylcarbamazine (DEC) is often accompanied with serious adverse events such as fatal encephalopathy, also loss of vision can occur if DEC is given to persons with active loiasis and onchocerciasis.[3] Furthermore, the use of Ivermectin (IVM) can result in severe encephalopathy and mortality in patients with a high burden of *Loa loa* infection.[4] Furthermore, the development of drug resistance in helminths necessitates the discovery of novel and safer anti-filarial drugs.[5] The use of medicinal plants for the treatment of parasitic diseases is becoming increasingly common in recent years as a method of avoiding the adverse effects of medication.[6]

The seeds of *Centratherum anthelminticum* (L.) (CA) Kuntze (scientific synonyms: *Veronia anthelmintica*), commonly known as black cumin, are widely used as spices in tropical countries. The CA seeds have a variety of pharmacological properties, such as anti-viral, anti-microbial, anti-fungal, and anti-diabetic activities.[7–9] For centuries, CA has been used as an efficacious anti-filarial and anti-helminthic remedy by ayurvedic practitioners in India. An earlier study has evaluated the effect of aqueous and alcoholic *C. anthelminticum* extracts on the filarial parasite *Setaria cervi*. The CA extracts inhibited spontaneous motility of *S. cervi* nerve-muscle preparations by decreasing the contraction amplitude and

Department of Biochemistry, Institute of Science, Banaras Hindu University, Varanasi, 221005, UP, India. E-mail: anchalsinghbhu@yahoo.com; anchalsingh@bhu.ac.in

frequency.[10] Although the anti-filarial effect of CA is known, there are no reports that provide a detailed explanation of its mechanism of action against the filarial parasites. Therefore, this work was conducted to evaluate the anti-filarial and adulticidal activity of CA extract against filarial parasite *Setaria cervi* using a combination of *ex vivo* biochemical, proteomics and *in silico* approaches.

2 Materials and methods

2.1. Parasites collection, culture and exposure to CA extract

The worms were procured as described previously[11] and brought to the laboratory in Kreb's–Ringer bicarbonate buffer (KRB) supplemented with streptomycin, penicillin, glutamine and 0.5% glucose (KRB maintenance medium). Further worms were incubated in KRB maintenance medium (KRBM) at 37 °C in a water bath for one hour before further use.[12] Equal numbers ($N = 6$) of adult female parasites were cultured in 20 mL of KRBM with varying doses of CA for 4 hours at 5% CO_2 at 37 °C and 95% humidity. Worms incubated in KRBM with Dimethyl sulfoxide (DMSO) 0.37% served as vehicle control. The movement of the treated worms was visually inspected by an investigator who was blinded to the experiment, and the motility was assessed as either positive or negative at hourly interval for a period of four hours and marked as either positive or negative (+/−) accordingly. The motility analysis was based on the movement score; a score of "+++++" indicates that the parasites are very active, a score of "+" that they are not very active, and a score of "−" that they are not moving.[11,13] In order to check the recovery, parasites were also transferred to new KRBM after 4 hours. The median lethal dose (LC_{50}) was determined by using OriginPro 2024 software. All the experiments were carried out in triplicates.[14]

Following treatment, the parasites were stored at −80 °C before subjecting them to further analysis.[13]

2.2. Effect of CA on parasite viability and production of reactive oxygen species (ROS)

The viability of control and CA treated *S. cervi* parasites were determined by MTT assay.[15] *S. cervi* worms were incubated in Phosphate Buffer Saline (PBS) medium containing 0.5 mg mL^{-1} MTT (3-(4,5-dimethylthiazol-2yl)-2,5-diphenyl tetrazolium bromide) for 2 hours at 37 °C in dark. Next, the worms were transferred into 200 μL DMSO and formazan crystals were solubilized. After 1 (one) hour of incubation, medium was carefully aspirated and absorbance (OD) of the solution was measured at 540 nm in a microplate reader (BioRad). For ROS production, the method of Sim Choi *et al.*[16] was followed with minor changes. The worms were incubated in 2% Nitro Blue Tetrazolium (NBT) solution for 1 hour at room temperature, followed by washing with PBS and methanol. In the next step, the formazan crystals were dissolved in 2 M KOH (prepared in DMSO) and the final absorbance was recorded at 620 nm in a microplate reader (BioRad).

2.3. DNA fragmentation analysis

The worms were homogenized 20 mM Tris buffer pH 8.0, 50 mM EDTA, 0.5% SDS, 100 mM NaCl, 1% β-mercaptoethanol,

and 0.1 mg mL^{-1} proteinase K, and then incubated at 55 °C for 3 hours. DNA was extracted using a 25 : 24 : 1 mixture of phenol, chloroform, and isoamylalcohol, followed by centrifugation at 10 000 rpm. Next the supernatant was treated with 3 M sodium acetate and 100% cold ethanol, the pellet was washed with 70% ethanol, and dissolved in 10 mM Tris–EDTA (TE) buffer (pH 8.0).[17] The isolated DNA sample was separated on a 1.8% agarose gel containing ethidium bromide, and images were recorded in a GelDoc system (Biorad, Hercules CA).

2.4. Assessment of NADPH oxidase activity

Both the control and treatment groups were homogenized separately in 50 mM phosphate buffer (pH 7.2), 0.25% SDS, and centrifuged for 10 min. at 600 g at 4 °C. The resulting supernatant (100 μL) was combined with 1 mM $MgCl_2$, 80 μM cytochrome c, and 2 mM sodium azide in a total volume of 1 mL. After adding 0.2 mM NADPH to start the reaction, the change in absorbance at 550 nm was measured.[18]

2.5. Determination of protein carbonylation (PC) and lipid peroxidation

Using 2,4-dinitrophenyl hydrazine (DNPH), protein carbonyl concentration was assessed in the control and CA treated worms.[19] Equal volumes of 10% cytosolic extract and cold trichloroacetic acid (TCA) were mixed and centrifuged at 6000 g for 5 minutes at 4 °C. Next, the pellet was treated with DNPH (10 mM), and kept in dark at room temperature for one hour with occasional vortexing. After one hour the mixture was centrifuged at 6000 g for 5 min, and 20% TCA was added. The pellet was washed with a mixture of ethanol and ethyl acetate (1 : 1) until the yellow tint vanished. 6 M guanidine hydrochloride was added to the pellet and the mixture was centrifuged at 6000 rpm for 5 min. at 4 °C. The molar extinction coefficient of 22 000 × 10^6 mM^{-1} cm^{-1} was used in calculations.

Assessment of lipid peroxidation of the control and treated worms was based on the levels of malondialdehyde (MDA). The reaction was started by adding 10% SDS to 300 μL of cytosolic extract to begin the reaction, which was then incubated at RT for 5 min. Next 600 μL of 20% acetic acid was added, followed by a second incubation at RT for 2 min, and finally 0.8% of 2-thiobarbituric acid (TBA) was added. In a water bath, the entire mixture was boiled for one hour.[20] Next, the mixture was centrifuged at 10 000 g for 5 min at 4 °C. The supernatant's absorbance was then measured at 532 nm to determine the amount of TBA reactive compounds. TBA was calculated using the molar extinction value of 1.53 × 10^5 M^{-1} cm^{-1}.

2.6. Preparation of *S. cervi* homogenate

The 10% w/v homogenate of adult female *S. cervi* was prepared in 100 mM Tris–HCl, pH 7.0 containing, 1 mM EDTA, and 1 mM phenylmethylsulphonyl fluoride (PMSF) using a motor-driven homogenizer (REMI type RQ127A) at 4 °C. The homogenate was centrifuged at 10 000 rpm for 15 min at 4 °C. Next, the clear supernatant was stored at −20 °C in aliquots. The protein was quantified by the Bradford's method and Bovine serum albumin was used as a standard.[13]

2.7. 2D gel electrophoresis

With a few modifications, 2D gel electrophoresis was carried out as previously described.[21,22] The *S. cervi* protein homogenate was treated with 4 : 1 (acetone : protein) volume of ice-chilled acetone and kept at −20 °C for 5 hours, followed by centrifugation at 10 000 rpm for 10 minutes at 4 °C. 200 μl of the rehydration solution (7 M urea, 2 M thiourea, 2% w/v CHAPS, 15 mM DTT, 0.5% v/v IPG buffer pH 3–10) was used to collect and rehydrate the pellet. For improved resolution, 11 cm IPG strips with pI values 3–10 were used for better resolution of samples. The isoelectric focusing (IEF) at 20 °C was carried out in a Protean IEF Cell (BioRad, United States) as per: 150 μA per strip for 15 min, then quickly ramping up to 8000 V for 2 hours and 8000 V for 20 000 V for 7 hours (with a limit of 50 μA per strip). Following IEF, 40 mM Tris–HCl buffer (pH 8.8) containing 6 M urea, 25% w/v glycerol, 2% w/v SDS, 1% w/v DTT, and 2.5% iodoacetamide was used to equilibrate the strips.[23] The second dimension was performed in 10% SDS PAGE. The gel was then stained with Coomassie Brilliant Blue G-250, (10% aluminum sulfate, 10% ethanol, 0.02% CBB G-250, and 2.5% orthophosphoric acid). Images of the gel were captured using a gel documentation system (Alpha Innotech, USA) and analyzed using PDQuest software (BioRad, USA). Three separate experiments were conducted to verify the reproducibility.[24]

2.8. High resolution accurate mass spectrometry analysis

The samples were reduced with 10 mM dithiothreitol (DTT) for 1 h followed by treatment with 2% iodoacetamide (IDA), with 50 mM NH_4HCO_3/50% acetonitrile (ACN) thrice for 10–15 min with gentle vortexing and incubation in dark. The samples were then digested with Trypsin (Trypsin gold Promega, USA) and incubated at 37 °C for overnight. The extracted peptides were lyophilized, desalted and stored at −80 °C till further use.[25] An Orbitrap Eclipse Tribrid Mass Spectrometer with nano-LC and UHPLC at Central Discovery Centre, Banaras Hindu University was used for peptide analysis. The samples were analyzed using a 120 min linear gradient of buffer B (80% Acetonitrile and 0.1% formic acid) at a flow rate of 0.300 μL min^{-1} and scanning was done in the range of 200–1600 m/z. The individual peptides MS/MS spectra were matched to the database sequence on Thermo Scientific™ Proteome Discoverer™ software. The samples were run in triplicates and abundance ratio value was set as ≥1.50 for upregulated and ≤0.667 for downregulated proteins respectively.[25,26] The statistical significance was evaluated using T-tests and the significance index was computed based on the corresponding P value, where a default threshold of $P < 0.05$ was employed.[25]

2.9. Gene ontology analysis

The UniProt database, available at https://www.uniprot.org/, was utilized to facilitate the investigation of the Gene Ontology (GO) annotation proteome. The UniProt IDs were obtained by searching the UniProt database for the corresponding protein's accession number. By using GO annotation, major proteins were classified into categories according to their biological processes (BP), cellular components (CC), and molecular function (MF). The MF, CC, and BP of proteins were then visualized or formed into networks using Cytoscape (http://www.cytoscape.org, version 3.1.1). For this investigation, only the primary network-forming proteins were chosen. Excel was then used to create histograms for the classification and display of the MF, CC, and BP of proteins.

2.10. Structure retrieval of filarial anti-oxidant proteins

Previously modelled structure of *W. bancrofti* glutathione *S*-transferase (GST) (5D73, DOI: https://doi.org/10.2210/Pdb5D73/pdb), *W. bancrofti* thioredoxin (TRx) (4FYUA, 10.2210/pdb4FYU/pdb) and *B. malayi* superoxide dismutase (SOD), (accession no. CTP82144.1) were previously constructed by our laboratory hence they were used as such for molecular docking.[27] The 3 dimensional structure of filarial glutathione peroxidase (GPx) could not be located in any databases hence sequence of *B. malayi* GPx was retrieved (PM0077541). The structure was modeled with LOMETS and validated using PROCHECK and Rampage server.[28] Further the 3D model for GPx was validated by ERRAT, ProSA, and ResProx server to determine its quality. The VADAR server was used to verify the hydrogen bond statistics and quality of the GPx models. The active site in the modelled 3D structure of GPx was predicted by Metapocket 2.0 server.[29]

2.11. *C. anthelminticum* extract preparation

The seeds of CA were purchased locally in Varanasi, Uttar Pradesh, India (between latitude 25.267878 and longitude 82.990494). Prof. Shashi Pandey, a taxonomist at the Botany Department, Institute of Science, Banaras Hindu University, made the botanical identification. 25 g of CA seeds were powdered under cold condition and defatted with *n*-hexane using a Soxhlet extractor. Thereafter the residue obtained was further fractionated with 250 mL of ethanol.[30] The crude fractions were collected, filtered and concentrated to dryness under reduced pressure in a rotary evaporator (<40 °C). Before treatment the dried powder was solubilized in DMSO. The total percent of DMSO was always ≤0.37% of KRBM and an equal volume of DMSO was added to the control flasks also.

2.12. FT-IR analysis of CA seed extract

A PerkinElmer Spectrum 65 Fourier Transform Infrared Spectrometer (FT-IR) was used to analyze the ethanolic extract of CA.[31] The spectra were gathered between 4000 cm^{-1} and 400 cm^{-1} wavelength. Signal to noise ratio of spectra was improved by 100 interferograms with a special resolution of 4 cm^{-1} average. Additionally, background spectra were captured under the same circumstances and subtracted from the sample spectra. The experiment was done in triplicates, and OriginPro 8.0 was used to pick and integrate peaks, identify features and label them after importing the original FT-IR

spectral files. Normalization and background removal was done to regulate the spectral quality.

2.13. UPLC-ESI-MS/MS analysis of *C. anthelminticum* extract

UPLC-ESI-MS/MS analysis was performed on Acquity Ultra Performance Liquid Chromatography Electrospray Ionization Tandem Mass Spectrometry. Chromatographic separation of CA seed extracts was performed using an ACQUITY UPLC, BEH C_{18} column, 35 °C. The mobile phase has two phases: A phase, methanol and water (5 : 95) and B phase methanol and water (95 : 5) with 0.1% formic acid. Mass Lynx 4.1 software was used for data collection and processing. Phytochemical software equipped with RIKEN tandem mass spectral database (ReSpect) was utilized for detailed analysis of UPLC-ESI-MS/MS data.[32]

2.14. Retrieval of ligand structures

CA bioactive compounds were selected for docking analysis based on UPLC-ESI-MS/MS data. Using Biovia Discovery Studio 3.5 (**https://discover.3ds.com**), the structures of the ligands were converted into PDB format which were retrieved from PubChem Database in SDF format.[33] Drug like behavior of CA bioactive substances was predicted using the Lipinski filter.[34] AdmetSAR server was used to forecast the Absorption,

Distribution, Metabolism, Excretion, and Toxicity (ADMET) properties of CA bioactive substances.[35]

2.15. Docking analysis

YASARA and PatchDock server were employed to perform docking analysis of filarial antioxidant proteins with CA bioactive compounds. The PatchDock server's default setting for the RMSD value for protein and ligand complexes was 1.5. Discovery Studio 3.5 was used to visualize the docked complexes. The parameters GSC (geometric shape complementary) score and AI (approximate interface) area were obtained from PatchDock server,[36] binding energy (kcal mol^{-1}) and dissociation constant (μm) as given by YASARA (Yet Another Scientific Artificial Reality Application) server were used for data interpretation.[37]

2.16. Molecular dynamics simulation analysis

Molecular dynamic simulation utilizing NAMD (Nanoscale Molecular Dynamics v 2.14) was used to assess the stability of the interaction between filarial antioxidant protein models and ligands.[27] The Open Babel Chemical Format Converter (**https://www.cheminfo.org/Chemistry/Cheminformatics/FormatConverter/index.html**) was used to convert the PDB
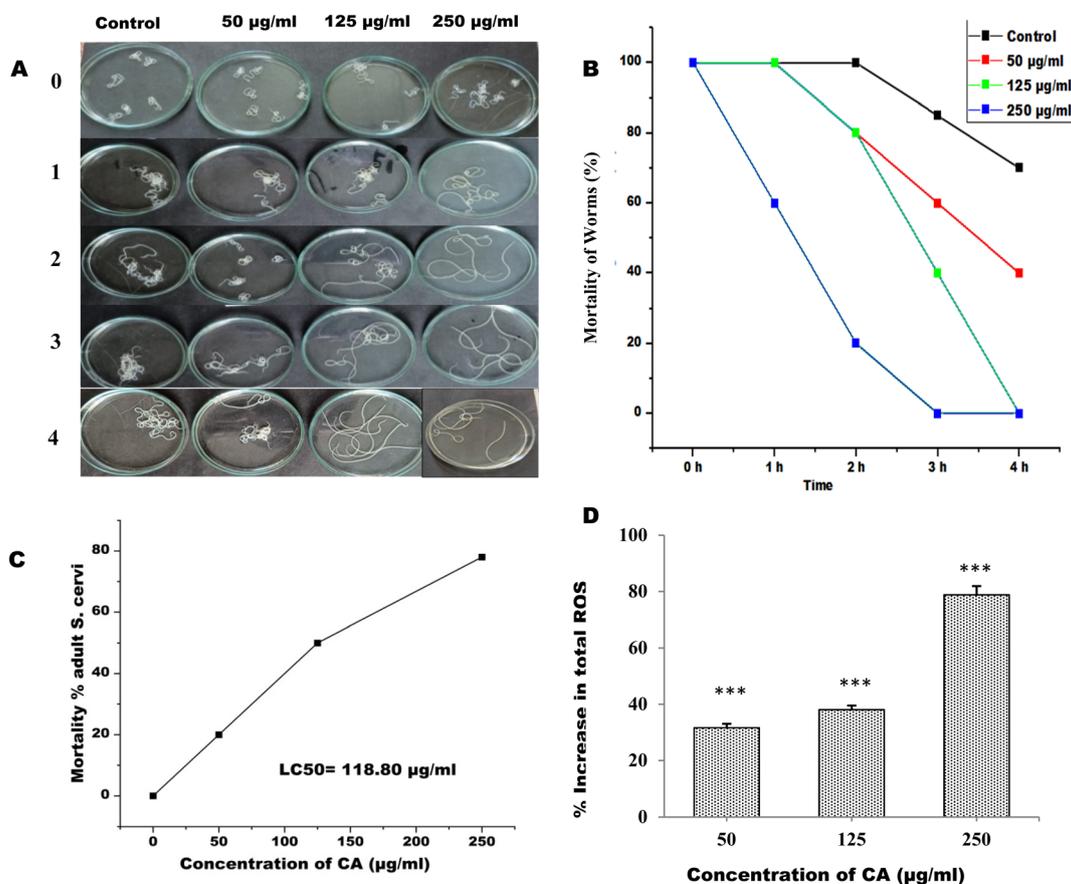
Fig. 1 Images of control and CA treated *S. cervi* (A) after 0, 1, 2, 3 and 4 h of treatment. (B) Motility of *S. cervi* worms after treatment was measured in percentage at hourly intervals. (C) LC_{50} value of CA for adult *S. cervi* (D) total ROS generation was measured using NBT as the substrate. ***$P < 0.001$, **$P < 0.01$, *$P < 0.05$. Values are mean $\pm$ SD of three experiments performed in triplicate.

RSC Advances

Table 1 Effect of *C. anthelminticum* ethanolic seed extract on the motility of *S. cervi*[a]

Sample	0 h	1 h	2 h	3 h	4 h	Recovery
Control	+++++	+++++	+++++	++++	+++	+++++
50 µg mL^{-1}	+++++	+++++	++++	+++	++	++++
125 µg mL^{-1}	+++++	+++++	++++	++	−	−
250 µg mL^{-1}	+++++	+++	+	−	−	−

[a] Motility of the incubated parasites was evaluated as − (0%), no movement; + (20%), least active; ++ (40%), less active; +++ (60%), moderately active; ++++ (80%), highly active; and +++++ (100%), very high active. Worms were transferred into fresh medium after 4 h and motility recovery in treated group was compared with respect to the control. Results are from three independent experiments performed in duplicates.

files of the CA compounds into Sybyl Mol2 files. Using the Sybyl Mol2 ligand modeler and the CHARMM-GUI input generator (**https://www.charmmgui.org/input**), PSF and

forcefield parameter values of CA bioactive compounds were selected. The VMD dispdev command was used to produce complexes of proteins and CA bioactive substances. In protein and CA bioactive compound complexes, the complexes were solvated in the *X*, *Y*, and *Z* axis in an orthorhombic water model with a distance of 10 Å. The complexes was also neutralized with 0.15 M NaCl and solvated by a TIP3P water box with a 5 Å layer of water in each direction. The PARAM SHIVAY supercomputing facility of IIT BHU was used to simulate molecular dynamics. Under 3D periodic boundary conditions, an MD simulation was run at 310 K temperature, 1000 steps, energy minimization, and 50 ns time trajectory. Root mean square deviation (RMSD), root mean square fluctuation (RMSF), radius of gyration (R_g), and solvent accessible area analysis (SASA) fluctuations were calculated during the simulation run and the findings were visualized by VMD.
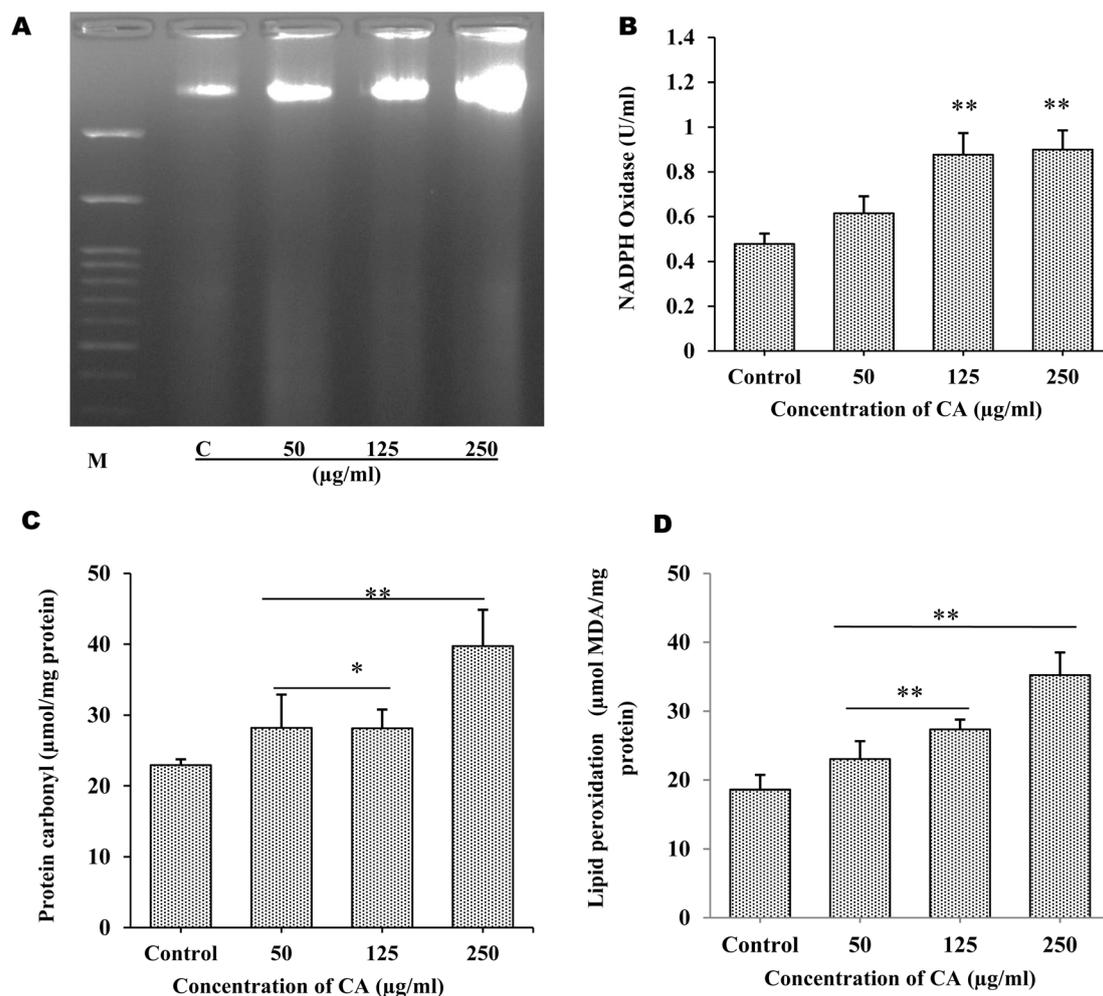
Fig. 2 Adult worms (*n* = 6) of equal size were exposed to CA extract, worms incubated in KRBM served as control (A) DNA fragmentation in adult female *S. cervi* after 4 h of treatment followed by DNA isolation. The isolated DNA from control and treated worms was run on 1.8% agarose gel. C: control, treated parasites (50, 125, and 250 µg mL^{-1} of CA extract) and M: marker (molecular weight 100–3000 bp). The activity of oxidative stress marker was checked as given in Method section (B) NADPH oxidase activity (unit per ml) (C) the protein carbonyl content is given as µmol mg^{-1} protein (D) lipid peroxidation in terms of µmol MDA/mg protein. Data expressed is mean ± SD of *n* = 3, *P* values <0.05 (*), <0.01 (**) were considered statistically significant.

2.17. Statistical analysis

Each experiment was run in triplicates and the data are shown as mean ± SD and were computed using the OriginPro 2023b (https://www.originlab.com/). Using GraphPad prism software 9.5.0, the Student's t-test was applied for the statistical significance between control and the CA-treated worms (*$p <$ 0.05, **$p <$ 0.01 and ***$p <$ 0.001).[25]

3 Results and discussion

3.1. *In vitro* effect of CA treatment on motility and viability of adult *S. cervi*

The adult female *S. cervi* were incubated in KRBM for 4 hours at 37 °C, with 5% CO_2 and 95% humidity in a carbon dioxide incubator. It was observed that the *S. cervi* parasites treated with CA concentration of ≥125 µg mL^{-1} were completely non-motile after 4 hours of incubation (Fig. 1A and B). The reduction in *S. cervi* motility was time and dose-dependent. After 4 hours of incubation, the adult parasites were transferred to fresh KRBM for 1 hour to check their recovery post CA treatment (Table 1). The worms treated with 50 µg mL^{-1} of CA were able to revive in the fresh medium, while the parasites treated with concentrations of 125 µg mL^{-1} and 250 µg mL^{-1} showed no evidence of recovery even after an hour of incubation. The lethal effect of CA appears to be of permanent nature at concentration >125 µg mL^{-1}. The viability was decreased to 80%, 50.33%, and 22% after 4 hours of 250 µg mL^{-1}, 125 µg mL^{-1}, and 50 µg mL^{-1} CA treatments respectively. The 50% lethal concentration (LC_{50}) was observed to be 118.80 µg mL^{-1} after 4 hours of treatment (Fig. 1C). The viability of *S. cervi* decreased as a function of concentration following CA treatment.

3.2. CA treatment induces ROS production and DNA fragmentation in adult *S. cervi*

The production of ROS by *S. cervi* worms during CA treatment was estimated by NBT assay. The intracellular ROS was significantly higher in CA treated parasites as compared to control worms. The ROS production increased by 31.64% in 50 µg mL^{-1} (P-value ≤0.001), 38.04% in 125 µg mL^{-1} (P-value ≤0.001), and 78.78% in 250 µg mL^{-1} (P-value ≤0.001) in treated parasites as compared to the control group (Fig. 1D). The effect of elevated ROS level on cellular DNA was assessed by the DNA fragmentation assay. The DNA fragmentation analysis revealed dose-dependent nucleosomal DNA destruction and the maximal DNA laddering was seen at CA concentration of 250 µg mL^{-1} whereas 50 µg mL^{-1} concentrations, fragmentation was the least (Fig. 2A). Previously CA and its bioactive compound vernodalin have been shown to induce high levels of ROS in melanoma and breast cancer cells[7,38] resulting in the apoptosis of the cancer cells. Since in our case too, the ROS was significantly higher after CA treatment causing a huge oxidative stress on the filarial parasites which could be a causative reason for the death of the parasites.

3.3. CA treatment leads to increase in oxidative stress in *S. cervi*

The major hallmarks of programmed cell death are DNA fragmentation and increase in the cellular levels of ROS. Therefore the alterations in the oxidative stress indicators such as, protein carbonyl (PC) level, lipid peroxidation, and NADPH oxidase activity were also examined. Using 125 µg mL^{-1}, and 250 µg mL^{-1} of CA seed extract, NADPH oxidase activity significantly increased by +82.05% ($p ≤$ 0.005), and +87.69% ($p ≤$ 0.005),
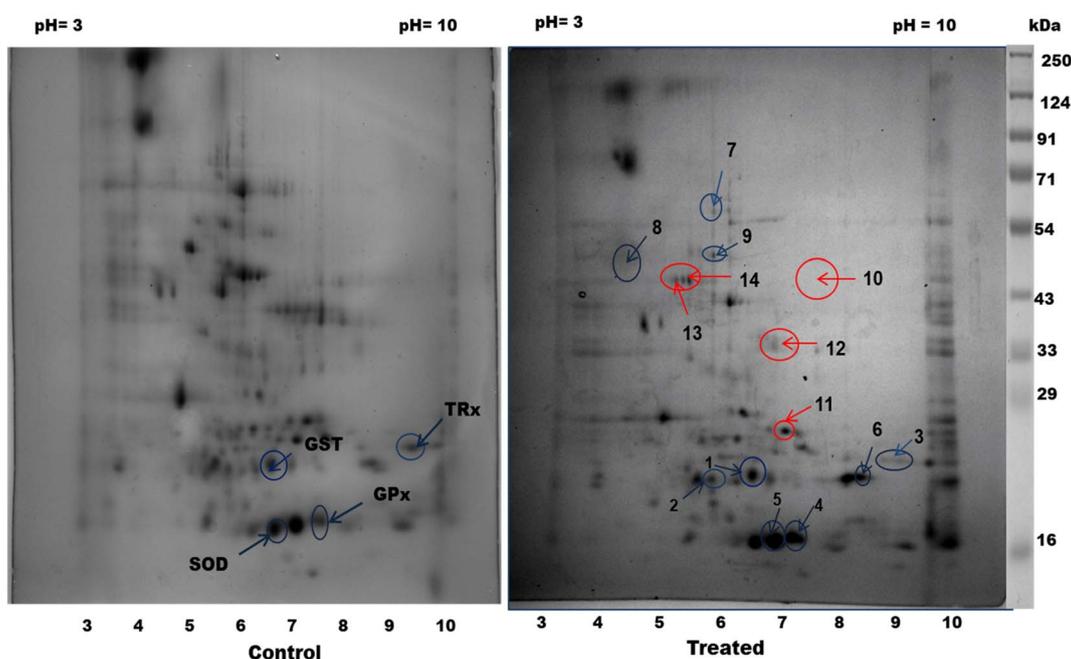
Fig. 3 Differential expression of proteins in cytosolic fraction of *S. cervi*: 2D gel electrophoresis analysis of total homogenate of control and CA treated parasites. Red arrow: downregulated; blue arrow: upregulated protein spots.

Table 2 List of upregulated proteins in CA treated vs. control groups

S. n.	Accession	Description	M_W [kDa]	Score sequest HT	Abundance ratio: (treated)/(control)	Abundance ratio P-value: (treated)/(control)
1	A0A3P7FFD1	Phosphoglucomutase (alpha-ᴅ-glucose-1,6-bisphosphate-dependent)	62.5	16.6	25.911	6.88338×10^{-15}
2	J9EA55	AV25 protein	20.4	4.24	12.106	2.55534×10^{-9}
3	A0A8L7T780	Transthyretin-like family protein	15.9	60.78	10.112	3.28489×10^{-8}
4	E3UV59	Glutathione S-transferase	24.1	5.48	7.910	0.004939501
5	A0A0J9Y0Q8	BMA-HIP-1	38.9	19.14	6.427	9.12162×10^{-6}
6	A0A1I8EK35	ʟ-Lactate dehydrogenase	35.7	156.75	4.506	0.000338363
7	O97149	Activation-associated secreted protein-1	24.6	13.85	4.493	0.000347 487
8	A0A4E9FMP9	Superoxide dismutase	25.1	30.99	4.25	0.572008685
9	J9APK4	Glutathione peroxidase	16.3	3.61	3.985	0.404530915
10	J9EFL6	Tropomyosin (fragment)	9.4	45.79	3.835	0.001389045
11	A0A1I8EE03	Elongation factor 1-alpha	50.8	212.39	3.543	0.002641362
12	Q04009	Myosin heavy chain	225.9	48.52	3.515	0.002810523
13	A0A8L7YQ50	Alanine transaminase	60.8	8.34	3.312	0.004447048
14	A0A1I8EW65	Succinate–CoA ligase [ADP/GDP-forming] subunit alpha, mitochondrial	37.8	49.34	3.262	0.004990625
15	A0A3P7G595	Thioredoxin domain-containing protein	9.3	16.85	2.971	0.009770672
16	J9E6J2	Transthyretin-like family protein	20.2	44.08	2.945	0.010383163
17	A0A3P7DHN6	60S ribosomal protein L27a	28.6	4.05	2.904	0.011454856
18	A0A4E9FP34	Peptidyl-prolyl cis–trans isomerase	18.5	44.37	2.809	0.014346473
19	J9ETG6	UMP-CMP kinase	22.2	10.53	2.69	0.019053637
20	J9EPU8	RNA transcription, translation and transport factor protein	28.5	8.4	2.678	0.019571524
21	A0A8L7T3Z0	BMA-ERP-1, isoform d	28.7	43.95	2.559	0.026113795
22	A0A3P7DF31	Myosin tail domain-containing protein	127.7	136.72	2.431	0.035547965
23	A0A4E9FKG6	Tropomyosin family protein	20.5	315.12	2.415	0.037035642
24	A0A1I8EKE6	Elongation factor 1-alpha	50.7	417.89	2.41	0.037422667
25	A0A1I8EC27	DB domain-containing protein	22.4	9.92	2.357	0.042620241
26	A0A0K0JX89	Tubulin alpha chain	45.1	3.8	2.333	0.045151395
27	J9EYX9	30S ribosomal protein S19e	16.9	9.65	2.312	0.047586267
28	J9EKD7	50S ribosomal protein L31e	12.9	17.96	2.289	0.050293391
29	S6FMC3	Triosephosphate isomerase	27.1	229.44	2.28	0.051511685
30	A0A0K0J057	BMA-CYC-2.2	12.2	62.71	2.207	0.061510051
31	A0A1I8ENA1	ATP-dependent RNA helicase	81	15.94	2.19	0.064165527
32	A0A4E9FD82	S-methyl-5′-thioadenosine phosphorylase	31.6	38.6	2.182	0.065381791
33	A0A3P7DLL1	Glutamate dehydrogenase [NAD(P)(+)]	60.5	590.15	2.178	0.06616905
34	J9B9B8	SWIB/MDM2 domain-containing protein	34.2	4.79	2.122	0.075918113
35	A0A4E9FEL1	Aconitate hydratase, mitochondrial	84.7	8.72	2.121	0.076134949
36	A0A1I9G417	Bm5160, isoform b	9	154.89	2.076	0.084986192
37	A0A0H5S2M8	Bm3307 (fragment)	228.9	81.5	2.072	0.085738954
38	A0A3P7FDU5	60S ribosomal protein L7a	31.1	35.42	2.069	0.086395097
39	A0A1I8EUR5	Malate dehydrogenase	38.4	163.96	2.053	0.08993189
40	A0A4E9FPQ9	Moesin/ezrin/radixin homolog 1	67.2	9.32	2.032	0.094605644
41	A0A4E9FDM3	Hypothetical RNA-binding protein T28D9.2 in chromosome II, putative	23.6	20.84	2.018	0.098165902
42	A0A4E9EPZ8	Troponin family protein	32	95.48	2.001	0.102260576
43	A0A0K0J070	60S ribosomal protein L38	8.2	91.98	1.958	0.113584457
44	A0A4E9FA37	Triosephosphate isomerase	27.1	277.16	1.923	0.123993316
45	A0A3P7DR94	Cysteine rich repeat family protein	137.9	4.07	1.89	0.134409097
46	A0A4E9EZP7	Arginine kinase	40.5	15.23	1.881	0.13745321
47	A0A3P7FEU7	Aminotransferase class I/classII domain-containing protein	47.4	26.82	1.876	0.139157966
48	A0A4E9FZS3	Sodium/potassium-transporting ATPase subunit alpha	111.1	20.35	1.87	0.141310621
49	J9EHH9	Uncharacterized protein	134.4	5.05	1.855	0.146485992
50	J9ELW9	Chaperonin GroL	61.4	750.65	1.854	0.14701626
51	A0A4E9FT05	Chloride intracellular channel exc-4(excretory canal abnormal protein4), putative	33.9	11.42	1.849	0.148646905
52	A0A4E9ESS7	Methionine aminopeptidase 2	46.7	28.36	1.841	0.151566548
53	J9BDB6	Uncharacterized protein	13.6	36.76	1.814	0.162075474

Table 2 (Contd.)

S. n.	Accession	Description	M_W [kDa]	Score sequest HT	Abundance ratio: (treated)/(control)	Abundance ratio P-value: (treated)/(control)
54	A0A0K0JCL5	Bm3963, isoform b	12.6	2.01	1.814	0.161884262
55	J9FAQ8	Cation-transporting P-type ATPase N-terminal domain-containing protein	10.5	2.17	1.809	0.163845709
56	J9ASR6	Mlp/crp family protein 1	14.5	38.31	1.807	0.164843254
57	A0A5S6PN68	Fumarate hydratase	54.3	639.19	1.804	0.166166117
58	A0A1I8ESR7	Glutathione-disulfide reductase	52.6	7.02	1.785	0.173902686
59	A0A3P7DIY7	Glyceraldehyde-3-phosphate dehydrogenase	36.2	503.05	1.785	0.173814354
60	A0A3P7EAK0	Ribosome maturation protein SBDS	33.5	13.53	1.783	0.17465467
61	A0A1I8ERE7	Protein disulfide-isomerase	59	26.5	1.764	0.183044436
62	J9ENJ4	Ribosomal protein L37ae	12.7	10.28	1.762	0.183809632
63	A0A1P6BM73	Succinate dehydrogenase [ubiquinone] iron–sulfur subunit, mitochondrial	31.7	24.6	1.76	0.184836825
64	A0A1I8EAU9	Ndr family protein	39	16.16	1.758	0.18598488
65	J9AQV1	Adenylate kinase isoenzyme 1	22.8	139.74	1.720	0.89073951
66	A0A1I8EX81	Galectin	36.7	63.54	1.712	0.208012151
67	A0A1I8F0A6	Vacuolar proton pump subunit B	57.6	10.7	1.708	0.209815911
68	J9B374	Sorting nexin-12	19	19.5	1.701	0.213465697
69	A0A3P7E0Z2	MICOS complex subunit MIC60	79.8	12.91	1.689	0.219699941
70	A0A1P6BMC5	Ribonucleoprotein	14	19.75	1.683	0.223170446
71	J9EY80	Translation elongation factor Tu	54	22.13	1.673	0.22834361
72	A0A0H5SBF4	Bm3026	15.4	22.27	1.671	0.22962774
73	A0A4E9EUM6	Methionine aminopeptidase	43.3	5.66	1.644	0.245122576
74	A0A0M4FXK5	Phosphoglycerate kinase (fragment)	29	257.43	1.644	0.245077256
75	A0A4E9FW13	Adenylosuccinate synthetase	52.7	26.35	1.639	0.248281406
76	A0A4E9FV29	Tubulin gamma chain	49.2	17.68	1.631	0.252845192
77	A0A0J9XNT3	40S ribosomal protein S27, putative; BMA-RPS-27	9.5	20.5	1.63	0.253758622
78	Q6H323	Protein disulfide-isomerase (fragment)	53.9	19.63	1.625	0.256455645
79	A0A3P7G9Q2	26S proteasome complex subunit dss-1	62.4	14.76	1.619	0.260540116
80	A0A4E9FND0	Transthyretin-like family protein	15.3	156.07	1.619	0.26040714
81	A0A4E9FP97	DUF19 domain-containing protein	40.8	8.39	1.608	0.267531713
82	A0A3P7FCC0	Peptidase S1 domain-containing protein	31.5	18.54	1.601	0.272003697
83	A0A0K0JWH8	BMA-HMG-1.1	10.3	92.09	1.6	0.272838833
84	A0A5S6PN83	Ubiquitin carboxyl-terminal hydrolase 7	127.3	10.1	1.593	0.277634590
85	A0A4E9FGM3	Calponin-homology (CH) domain-containing protein	15.5	482.63	1.590	0.710268997
86	J9ES30	Cytoplasmic tRNA 2-thiolation protein 1 (fragment)	27.8	5.37	1.577	0.288359931
87	J9FJW2	60S ribosomal protein L12	31.1	93.71	1.576	0.288749514
88	A0A4E9FAX4	Hypothetical RNA-binding protein T28D9.2 in chromosome II, putative	45.5	8.2	1.576	0.288804578
89	A0A4E9FMS4	TATA-binding protein interacting (TIP20) domain-containing protein	142.8	10.07	1.564	0.297346175
90	A0A1I8EJ18	BAR domain-containing protein	34	77.51	1.563	0.297723468
91	J9FEN6	Succinate–CoA ligase [ADP-forming] subunit beta, mitochondrial	47.4	15.9	1.544	0.3118908
92	A0A4E9ESV3	Guanine nucleotide-binding protein subunit gamma	7.5	4.99	1.542	0.313185891
93	A0A1I8ETH8	GDP-L-fucose synthase	54.4	12.87	1.537	0.317223493
94	A0A4E9FBF2	Peripheral subunit-binding (PSBD) domain-containing protein	35.5	10.11	1.527	0.324770277
95	A0A4E9ER74	Uncharacterized protein	226	61.89	1.527	0.324530557
96	A0A5S6PLZ5	FAD_binding_2 domain-containing protein	56.8	76.37	1.518	0.331946859
97	A0A0I9NBF1	BMA-SNR-2	18.1	17.01	1.517	0.332302623

respectively (Fig. 2B). Superoxide anions are produced, when active NADPH oxidase transfers electrons to oxygen, which in turn may cause production of H_2O_2 and other toxic reactive oxygen species leading to disruption of mitochondrial membrane. The oxidative damage production by elevated superoxide anions was assessed by examining the PC content

Table 3 List of down-regulated proteins CA treated vs. control groups

S. n.	Accession	Description	M_W [kDa]	Score sequest HT	Abundance ratio: (treated)/ (control)	Abundance ratio P-value: (treated)/ (control)
1	J9FES9	Proteasome subunit alpha type (fragment)	24.7	187.5	0.669	0.317621517
2	J9FGQ7	MPN domain-containing protein	38.2	2.44	0.669	0.318789073
3	Q962A2	Translationally-controlled tumor protein homolog	20.8	85.57	0.66	0.302533179
4	J9DX04	RRM domain-containing protein (fragment)	6.7	5.6	0.658	0.29902988
5	A0A4E9F9C9	SGS domain containing protein	23	52.1	0.658	0.30006964
6	A0A3P7GA46	SH3 domain-containing protein	73.4	16.78	0.655	0.294743553
7	A0A1I8EEX0	Skp1-related protein	25.6	9.09	0.653	0.291820357
8	J9AKD6	26S protease regulatory subunit 8	29.8	42.72	0.652	0.289955506
9	A0A3P7GHM4	Vesicle-fusing ATPase	91.6	687.71	0.649	0.283644745
10	A0A1I8EG93	RuvB-like helicase	47.4	13.63	0.646	0.278619261
11	A0A8L7TJD2	UNC-52/perlecan, putative	375	10.96	0.641	0.27153754
12	A0A3P7FIZ2	Proteasome subunit alpha type	29	37.22	0.634	0.259568518
13	A0A4E9EWP4	ATP-dependent 6-phosphofructokinase	89.6	32.66	0.633	0.258764632
14	J9EVC3	Protein serine/threonine phosphatase 2C C-terminal domain-containing protein (fragment)	12.4	35.48	0.633	0.258401234
15	A0A4E9FBQ2	Trans-ketolase, putative	67.2	159.55	0.631	0.254455621
16	A0A3P7DP86	Uncharacterized protein	8.5	64.05	0.63	0.25304265
17	A0A5S6PC29	VWFA domain-containing protein	530.4	2.39	0.628	0.251074583
18	J9ENW2	Uncharacterized protein	13.8	6.32	0.623	0.241800228
19	J9FG14	Heat shock 70 protein (fragment)	67.8	847.76	0.623	0.242147498
20	A0A4E9FKH9	TPR domain containing protein	30.5	49.27	0.616	0.231755568
21	J9FBW7	Small heat shock protein	17.8	20.23	0.613	0.226798658
22	J9EFE8	Profilin	14.1	9.32	0.612	0.225932411
23	A0A1I8EI05	Twitchin	752.9	31.93	0.599	0.206227775
24	A0A0H5S9A3	Dihydrolipoyllysine-residue succinyl transferase component of 2-oxoglutarate dehydrogenase complex, mitochondrial	51.2	18.03	0.597	0.203409966
25	A0A0K0J9J7	60S ribosomal protein L35a	14.2	14.19	0.596	0.202731388
26	A0A4E9EZ61	Ribosomal protein L10e/L16 domain-containing protein	24.7	10.63	0.593	0.198052286
27	A0A4E9FBN8	Cytoplasmic intermediate filament protein, putative	67.8	262.21	0.59	0.19310016
28	A0A1I9G5N0	Bm898 (fragment)	4.3	11.34	0.577	0.176269485
29	A0A0J9Y2D9	BMA-SEM-5	23.5	21.62	0.569	0.165095268
30	A0A4E9EXP0	Uncharacterized protein	47.8	86.79	0.569	0.165994255
31	A0A5S6PR17	BMA-SRAP-1	211.8	13.27	0.565	0.159960888
32	A0A3P7DJL2	SHSP domain-containing protein	19.9	16.54	0.564	0.159719255
33	A0A0K0J064	Mitochondrial import inner membrane translocase subunit	10.6	36.55	0.556	0.149230289
34	J9BHI4	Prefoldin	18.2	2.95	0.554	0.14646369
35	A0A1I9G512	Bm2039, isoform c	50.8	14.3	0.552	0.144422143
36	A0A8L7SNZ6	Transcriptional activator protein Pur-alpha	29.4	14.53	0.551	0.142684051
37	A0A4E9FBQ6	NADP-dependent oxidoreductase domain-containing protein	36.3	7.59	0.546	0.137456776
38	A0A1I8EXK7	Oxoglutarate dehydrogenase (succinyl-transferring)	112.5	5.65	0.544	0.134605963
39	A0A4E9FE28	V-type proton ATPase subunit F	13.6	9.24	0.543	0.134175691
40	A0A8L7SX06	Fatty acid synthase	138.4	8.64	0.543	0.133977568
41	A0A0J9XPL7	BMA-LSM-7, isoform a	11.3	6.38	0.53	0.119384074
42	A0A0J9XYB9	BMA-DNJ-13, isoform c	36.8	20.03	0.527	0.115927318
43	A0A0J9XRU7	60S ribosomal protein L35	19	9.51	0.524	0.113361363
44	A0A1I8EDE6	Proteasome endopeptidase complex	26.1	18.22	0.523	0.112421588
45	J9FF58	Laminin subunit gamma-1 (fragment)	183.1	10.78	0.521	0.110046266
46	A0A0J9XLH0	Bm9133	26.6	21.79	0.521	0.109601854
47	A0A7I4NJV0	ATP-dependent (S)-NAD(P)H-hydrate dehydratase	34.2	29.92	0.515	0.104291209
48	J9EGA5	Uncharacterized protein (fragment)	8.8	99.86	0.511	0.099662931
49	A8Q043	cAMP-dependent protein kinase regulatory chain, putative	7.2	34.74	0.501	0.091034522
50	J9EJZ2	Proliferating cell nuclear antigen	29.1	24.21	0.501	0.091036289
51	J9F0I0	Clathrin light chain	22.8	16.91	0.486	0.077156737
52	A0A4E9EVU8	Uncharacterized protein	58	17.39	0.485	0.077007995
53	A0A8L7SQJ2	Glutamine synthetase	41.2	19.22	0.478	0.071305005
54	A0A4E9FH92	RRM domain-containing protein	42.2	10.62	0.475	0.06861159
55	A0A4E9FEZ1	Vitellogenin domain-containing protein	361.1	10.63	0.473	0.06696446
56	A0A4E9FBY7	Proteasome alpha-type subunits domain-containing protein	27.7	67.83	0.472	0.066088914
57	A0A0K0JIQ0	Bm5388, isoform a	19.4	1.89	0.466	0.061851423
58	J9FCT2	Mannose-6-phosphate isomerase	45	3.59	0.452	0.052220282

Table 3 (Contd.)

S. n.	Accession	Description	M_W [kDa]	Score sequest HT	Abundance ratio: (treated)/(control)	Abundance ratio P-value: (treated)/(control)
59	A0A3P7E5V5	Integrin beta N-terminal domain-containing protein	13.7	18.4	0.449	0.05058465
60	J9F5C4	Mitochondria bc1 complex core subunit 1 (fragment)	50.3	5.48	0.447	0.049436044
61	J9ARA6	40S ribosomal protein S8 (fragment)	17.2	80.97	0.438	0.044081236
62	A0A0J9XNT1	Bm255	9.2	52.04	0.436	0.042833626
63	A0A4E9F8W1	UBC core domain-containing protein	19	7.45	0.414	0.031326666
64	A0A1I9GCP6	Bm9018	138.4	7.98	0.4	0.025577555
65	A0A5S6PPU7	BMA-ALX-1	75.9	19.01	0.399	0.025295669
66	A0A0J9Y905	BMA-TLN-1, isoform a	278.1	38.09	0.398	0.024679215
67	A0A1I8EBP1	RRM domain-containing protein	40.7	21.66	0.366	0.014543053
68	J9BBS8	NADAR domain-containing protein	36.5	28.47	0.366	0.014527273
69	A0A3P7EB04	Uncharacterized protein	28	12.76	0.364	0.013891842
70	A0A4E9FSQ9	Leucine rich repeat family protein	27.6	9.56	0.358	0.012376684
71	J9FDW3	Transketolase	67.3	133.19	0.348	0.010169759
72	J9DT68	Uncharacterized protein	10.5	8.39	0.348	0.01018951
73	A0A8L7SNS8	Adenosylhomocysteinase	48.1	21.63	0.346	0.009749431
74	A0A5S6PIB0	BMA-PQN-22	84.6	11.12	0.342	0.009029136
75	A0A5S6P7N8	Uncharacterized protein	91	5.47	0.325	0.006333444
76	A0A1I8EWK5	BSD domain-containing protein	38.7	2.41	0.304	0.003846617
77	A0A0H5S5L6	BMA-ALP-1	67	5.34	0.3	0.003448479
78	A0A5S6PX95	Bm8873, isoform c	100.3	21.58	0.297	0.003182232
79	A0A3P7ETZ6	PDZ domain-containing protein	44.7	3.84	0.289	0.002555259
80	J9E3C5	Uncharacterized protein	7	5.69	0.284	0.002213946
81	A0A4E9FE79	Proteasome subunit beta type 2, putative	17.9	4.54	0.27	0.001482822
82	A0A5S6PAI6	Uncharacterized protein	24.6	5.79	0.244	0.000627717
83	A0A3P7FJZ7	Uncharacterized protein (fragment)	50.6	8.01	0.132	9.35986×10^{-7}
84	A0A1I8EP56	60S ribosomal protein L30	12.3	38.81	0.013	1×10^{-17}
85	A0A3P7DU85	Coatomer subunit beta	107.2	2.38	0.01	1×10^{-17}
86	A0A4E9EXG9	RWD domain-containing protein	29.9	2.84	0.01	1×10^{-17}
87	J9EMX1	Eukaryotic translation initiation factor 3 subunit K	18.8	3.34	0.01	1×10^{-17}
88	A0A3P7DVD5	Activator of Hsp90 ATPase AHSA1-like N-terminal domain-containing protein	40.3	1.76	0.01	1×10^{-17}

and malondialdehyde levels. With CA treatment, PC content was shown to significantly increase by almost +27.01% ($p \leq$ 0.05), and +73.31% ($p \leq$ 0.005), in 125 μg mL^{-1} and 250 μg mL^{-1} respectively (Fig. 2C). Similar to the malondialdehyde levels, a rise in lipid peroxidation of about +47.1% ($p \leq$ 0.005), and +0.895% ($p \leq$ 0.005) fold change was observed in 125 μg mL^{-1} and 250 μg mL^{-1} respectively in CA treated worms in comparison to control parasites (Fig. 2D). The exposure of S. cervi to CA extract led to a significant increase in the lipid peroxidation and protein oxidation.

3.4. Proteome profiling by 2D electrophoresis and HRAMS analysis

Next, proteomic profiling by 2D electrophoresis and HRAMS analysis was applied to investigate the effect of CA treatment on the filarial parasites. Upon exposure of S. cervi worms to 250 μg mL^{-1} CA extract, a significant alteration in the proteomic profile was observed with respect to the control worms. A total of 155 spots in control and 131 spots in CA treated parasite were

observed in the proteome profiles after 2D gel electrophoresis. The PD-quest analysis identified 16 upregulated and 30 down-regulated proteins (Fig. 3). The Pearson correlation coefficient between the treated and control samples were observed at 0.448.

The HRAMS proteome profiling data was analyzed using the Thermo Scientific™ Proteome Discoverer™ software. The analysis of protein expression alteration was analyzed on the basis of abundance ratio. A threshold value of 0.67 was established for downregulated proteins, whereas a cut-off value of 1.5 was determined for upregulated proteins.[23] A total of 185 proteins were identified as differentially expressed following, CA exposure, as indicated in Tables 2 and 3. Among these proteins, 97 were found to be considerably upregulated, while 88 were significantly downregulated.

After CA treatment the levels of detoxifying enzymes such as glutathione S-transferase (GST), superoxide dismutase (SOD), thioredoxin, glutathione peroxidase and glutathione reductase were significantly increased. These enzymes play a crucial role in scavenging oxidants and serve as the parasites' primary defense
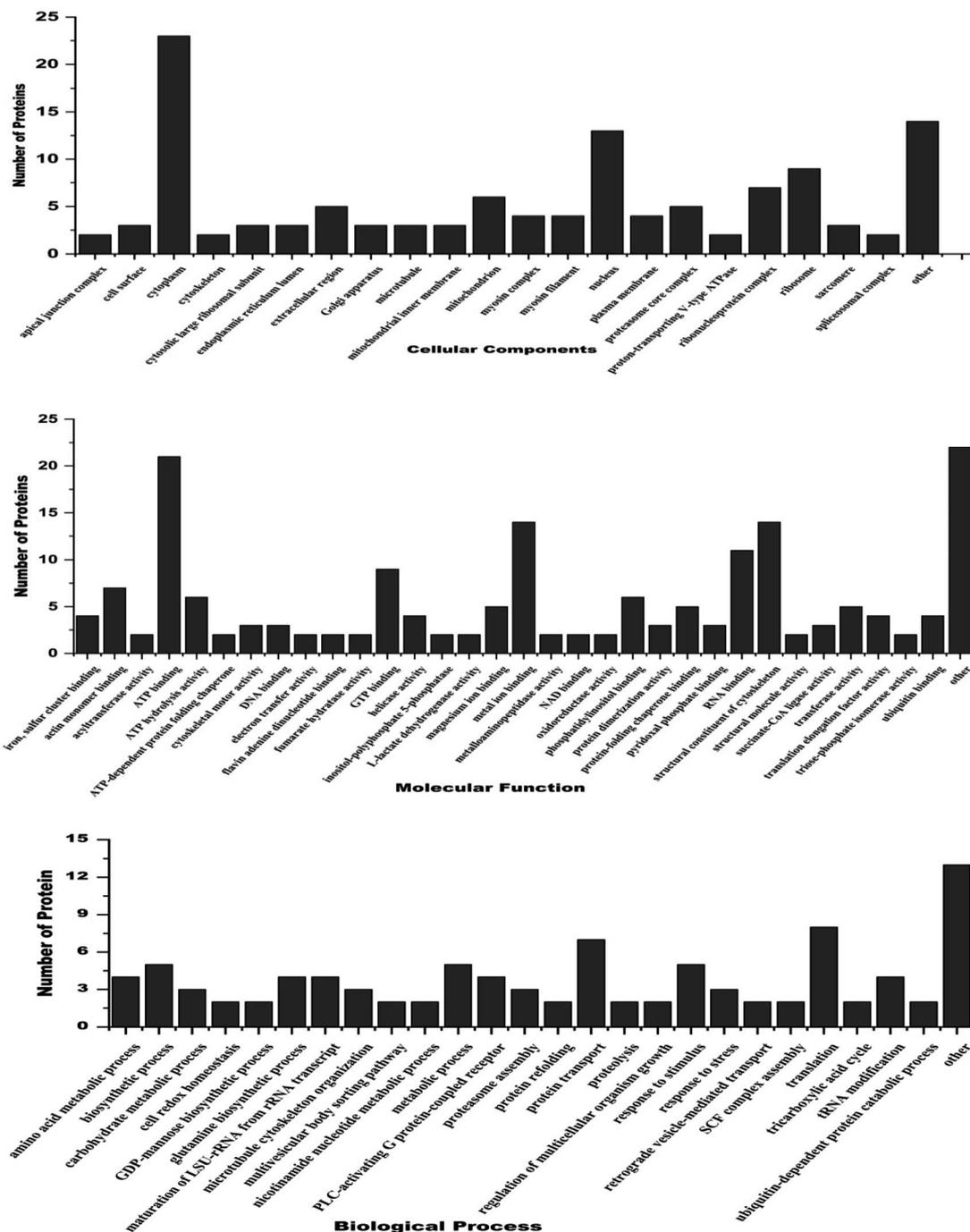
Fig. 4 Gene ontology analysis of differentially expressed proteins belonging to 3 major classes *i.e.* cellular component, molecular function and biological processes.

mechanism. The enzymes GST and SOD have a role in the metabolism of xenobiotics and their overexpression indicates an enhanced requirement for detoxification in CA treated parasites.

The expression of key components of the cytoskeletal structure, tropomyosin, myosin family proteins, tubulin, and moesin/ezrin/radixin (MER) homolog-1 was increased in the

filarial worms treated with CA. Myosin is the molecular component responsible for the contraction of sarcomeres and has the ability to convert chemical energy into mechanical energy. Moesin/ezrin/radixin homolog-1 facilitates the interaction of plasma membrane and filamentous actin, thus facilitating the cell cortex stability. The MERs control the signaling

pathway by binding transmembrane receptors and connecting them to downstream signaling components and the over-expression of these proteins could be correlated to significant alterations in the cytoskeleton of the parasite.[39]

The glycolytic enzymes enolase, triose phosphate isomerase, glyceraldehyde 3 phosphate dehydrogenase, and phosphoglycerate kinase were identified among the major upregulated proteins. Several enzymes involved in the energy metabolism such as phosphoglucomutase, ʟ-lactate dehydrogenase, succinate CoA ligase subunit alpha, triose phosphate isomerase, BMA-CYC-2.2, aconitate hydratase, malate dehydrogenase, glyceraldehyde-3-phosphate dehydrogenase, succinate dehydrogenase, phosphoglycerate kinase, were significantly upregulated after CA treatment. Some of these

enzymes are part of TCA cycle and glycolysis while BMA-CYC-2.2 is a component of the oxidative phosphorylation machinery. The upregulation could be due to increased demands for energy in CA treated parasites. Another highly upregulated protein was the transthyretin-like family protein molecular weight 15.9 and 20.2, which is involved in the apoptotic process of corps engulfment. The transthyretin-like family protein has been shown to have neuroprotective role as it protects dopaminergic neurons against degradation caused by oxidative stress.[40]

The major protein degradation pathways involves ubiquitin proteasome system involving proteasome subunit alpha type fragment (J9FES9), proteasome subunit alpha type subunit (A0A4E9FBY7), proteasome endopeptidase complex,

Table 4 Qualitative and quantitative output of CA ethanolic seed extract by negative ion mode liquid chromatography–mass spectroscopy

S. n.	Name of compound	Retention time (min)	Theoretical mass	Molecular formula	DB diff[a] (ppm)
1	CDP-DG (12 : 0/12 : 0)	15.875	840.3915	$C_{36}H_{65}N_3O_{15}P_2$	1187.08
2	Quinic acid	1.202	192.0596	$C_7H_{12}O_6$	19.47
3	Gentisic acid	2.028	154.0236	$C_7H_6O_4$	19.45
4	2-Acetylthiophene	4.724	126.0116	C_6H_6OS	18.86
5	*Trans*-chlorogenic acid	3.526	354.0897	$C_{16}H_{18}O_9$	15.19
6	Vanillin	5.639	152.0453	$C_8H_8O_3$	13.41
7	Soraphen A	14.703	520.2982	$C_{29}H_{44}O_8$	10.36
8	3-Acetyl-6-methoxybenzaldehyde	6.897	178.0612	$C_{10}H_{10}O_3$	9.85
9	IAA/3-indoleacetic acid	7.011	175.0617	$C_{10}H_9NO_2$	9.44
10	Irisolidone 7-*O*-glucuronide	5.948	490.1064	$C_{23}H_{22}O_{12}$	9.62
11	Flavine mononucleotide (FMN)	5.999	456.1006	$C_{17}H_{21}N_4O_9P$	8.85
12	4-Methoxycinnamoyloleanolic acid methyl ester	18.566	630.4232	$C_{41}H_{58}O_5$	8.29
13	3-Carboxyethenyl-3,5-cyclohexadiene-1,2-diol	8.308	182.0564	$C_9H_{10}O_4$	8.22
14	3-Methylindolepyruvate	10.651	217.0724	$C_{12}H_{11}NO_3$	7
15	3-*O*-Methylquercetin	9.393	316.0562	$C_{16}H_{12}O_7$	6.54
16	4-Dodecylbenzenesulfonic acid	19.63	326.1895	$C_{18}H_{30}O_3S$	6.4
17	Annotemoyin 1	20.124	564.4722	$C_{35}H_{64}O_5$	6.39
18	PG(16 : 1(9Z)/16 : 0)	19.087	720.4896	$C_{38}H_{73}O_{10}P$	6.26
19	Theasapogenol E	19.641	504.342	$C_{30}H_{48}O_6$	6.18
20	Dihydroxy-epoxyoctadecanoate	9.902	330.2386	$C_{18}H_{34}O_5$	6.18
22	Podorhizol beta-ᴅ-glucoside	7.221	578.1964	$C_{28}H_{34}O_{13}$	6.14
23	15-*O*-demethyl-dideoxydihydro-striatin C	15.039	434.2644	$C_{25}H_{38}O_6$	5.57
24	Ascorbyl stearate	10.851	442.2906	$C_{24}H_{42}O_7$	5.52
25	Avocadene 2-acetate	12.222	328.2596	$C_{19}H_{36}O_4$	5.5
26	Stypandrol	10.921	430.1393	$C_{26}H_{22}O_6$	5.48
27	RU 5135	13.253	304.2135	$C_{18}H_{28}N_2O_2$	5.3
28	Beta-obscurine	16.561	272.1877	$C_{17}H_{24}N_2O$	4.41
29	MG(15 : 0/0 : 0/0 : 0)	14.437	316.26	$C_{18}H_{36}O_4$	4.38
30	Carbenicillin	1.275	378.0869	$C_{17}H_{18}N_2O_6S$	4.32
31	Dibutyl decanedioate	13.252	314.2444	$C_{18}H_{34}O_4$	4.32
32	LysoPE(18 : 1(11Z)/0 : 0)	18.424	479.2995	$C_{23}H_{46}NO_7P$	3.61
33	*N*-undecylbenzenesulfonic acid	18.137	312.1748	$C_{17}H_{28}O_3S$	3.51
34	LysoPE(0 : 0/18 : 2(9Z,12Z))	15.105	477.2839	$C_{23}H_{44}NO_7P$	3.4
35	2-(Methylthiomethyl)-3-phenyl-2-propenal	3.746	192.0603	$C_{11}H_{12}OS$	2.98
36	Isopetasoside	15.16	396.2142	$C_{21}H_{32}O_7$	1.63
37	*N*-adenylyl-ʟ-phenylalanine	1.276	494.131	$C_{19}H_{23}N_6O_8P$	1.09
38	*S*-nitroso-ʟ-glutathione	9.159	336.0738	$C_{10}H_{16}N_4O_7S$	0.64
39	Mytilin A	5.385	332.1219	$C_{13}H_{20}N_2O_8$	0.27
40	Remifentanil	10.823	376.1997	$C_{20}H_{28}N_2O_5$	0.2

[a] (ppm) parts per million.

proteasome alpha-type subunits domain-containing protein, proteasome subunit beta type 2, and RWD domain-containing protein was highly downregulated. This system is responsible for degradation of more than 80% of the cellular proteins and is also actively involved in other cellular processes like apoptosis, control of cell-cycle progression and metabolic regulation.[41,42]

Harnessing the proteasome's destructive force to selectively degrade the drivers of human disease, has opened up a new and fascinating field of drug discovery. For example, targeted immunoproteasome inhibition has excellent clinical efficacy for autoimmune disease and inflammation and proteasome inhibitors could be used as innovative therapies for malaria and other microbes.[43] Also the heat shock proteins SHSP domain-containing protein and activator of Hsp90 ATPase AHSA1-like N-terminal domain-containing protein were highly downregulated. In another study, similar downregulation of HSPs was correlated with the death of filarial parasites.

The versatile central factor Proliferating Cell Nuclear Antigen (PCNA) was highly downregulated after treatment with CA seed extract in filarial parasites. The downregulation of PCNA after CA treatment could be one of the major factors for death of the filarial parasites. The PCNA encircles DNA, and act as proclivity factor in DNA replication.[44] PCNA forms the protein complexes in base excision repair, nucleotide excision repair, mismatch repair, homologous recombination, and cell cycle progression. Several researchers have established the fact that inhibition of PCNA could be a successful therapeutic strategy for treatment of cancer.[45]

The CA treated worms showed reduced expression of coatomer subunit β (abundance ratio *P*-value 0.01), low levels of coatomer leads to the fragmentation of Golgi apparatus, suppression of autophagy and cell death. It was also observed that many crucial enzymes such as adenosylhomocysteinase, transketolase, mannose-6-phosphate isomerase, and fatty acid synthase were significant downregulated, thus severely affecting the survival of the filarial worms.

3.5. Gene ontology and functional classification of differentially expressed proteins

Gene ontology annotation analysis for the most significant Differentially Expressed Proteins (DEPs), categorized by their molecular function, cellular components and biological process is shown in Fig. 4. Regarding molecular function, the main DEPs were involved in ATP binding, metal ion binding, GTP binding, ATP hydrolysis activity, actin monomer binding, oxidoreductase activity, protein folding, chaperone binding, RNA binding, transferase activity, and cytoskeletal motor activity as structural constituents of chromatin. The major DEPs in the biological processes category were mostly involved in tRNA processing, biosynthetic processes, metabolic activities, protein transport, tricarboxylic acid cycle, reaction to stimulus, glutamine biosynthesis processes, SCF complex assembly, translation process, and stress response. The biological components that showed substantial enrichment were the cell surface, nucleus, plasma membrane, cytoplasm, mitochondria, ribonucleoprotein complex, nucleosome, ribosomal protein, extracellular matrix, and spliceosome complex. Proteomic analysis showed that treating filarial worms with CA led to the suppression of many proteins involved in energy metabolism, signal transduction, stress response, chaperone proteins, and highly antigenic proteins.

3.6. FT-IR spectral analysis of CA ethanolic extract

FT-IR spectra of biological samples are typically performed in the range of 4000 to 400 cm^{-1} to identify functional groups of the active components by observing the emitted peaks in the infrared radiations. The spectrum pattern from the CA seed extract was observed at 602, 745, 1021, 1117, 1236, 1428, 1446, 1603, 1627, 2359, 2930, and 3352 cm^{-1}, respectively.
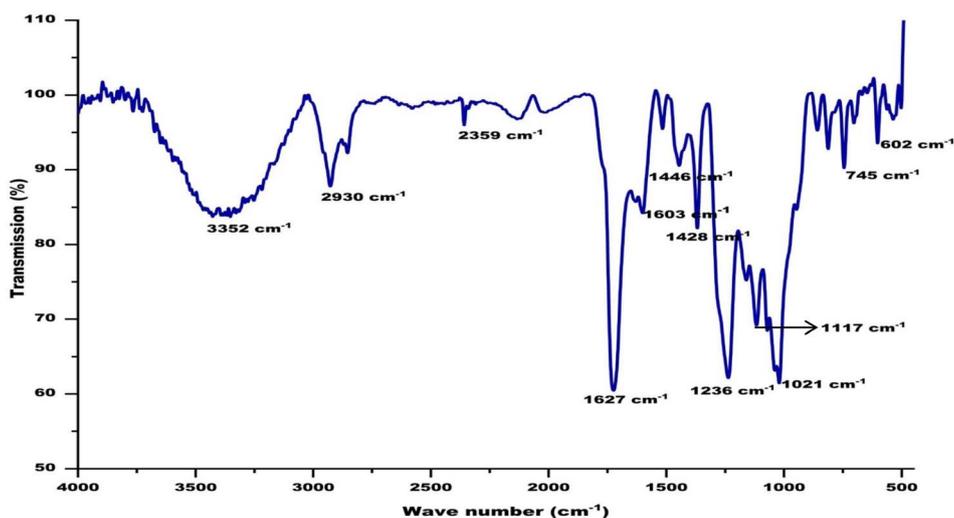

Fig. 5 Fourier-transform infrared spectroscopy analysis of ethanolic extract of CA.

Table 5 Bioactive compounds identified in ethanolic extract of CA by LC–ESI-MS/MS used for docking analysis

S. n.	Compounds name	RT (min)	Formula	M_W	Fragmentation profile (m/z)	DB diff[a] (ppm)
1	3-O-methylquercetin	9.393	$C_{16}H_{12}O_7$	316.05	207.0644 243.0273 255.0285 271.0234 300.0251 301.0295 315.0483 329.2307 395.0819	6.54
2	4-Methoxycinnamoyloleanolic acid methyl ester	18.566	$C_{41}H_{58}O_5$	630.42	325.1836 689.4342 690.434 719.4857	8.29
3	Podorhizol β D-glucoside	7.221	$C_{28}H_{34}O_{13}$	578.19	160.839 162.8346 195.8088 255.0482	6.14
4	RU5135	13.253	$C_{18}H_{28}N_2O_2$	304.21	129.0904 183.138 295.2262 296.2199 313.2369 314.2401	5.30
5	Soraphen A	14.703	$C_{19}H_{44}O_8$	520.29	277.2167 313.2366 403.2242	10.36
6	Vanillin	5.639	$C_8H_8O_3$	152.04	108.0196 109.0253 137.0221 151.0373 187.095 197.8061 262.065	13.41
7	Quinic acid	1.202	$C_7H_{12}O_6$	192.39	191.0524 192.0555 193.0577 195.0473 317.0493 377.0802 379.0777 539.1314	19.47
8	Gentisic acid	2.028	$C_7H_6O_4$	154.02	109.0266 110.0305 153.0165 175.0571 218.1004 282.0811	19.45
9	Beta-obscurine	16.561	$C_{17}H_{24}N_2O$	272.1877	331.201 332.2001 333.2019 367.1791 368.1794 369.1708 370.176	4.41
10	Carbenicillin	1.275	$C_{17}H_{18}N_2O_6$ S	377.08	191.0508 192.0493 377.0772 379.0766	4.32

[a] (ppm) parts per million.

The small sharp peak at 602 corresponds to the aromatic H-out of plane bending. Several small peaks in the range of 729–759 correspond to the C–C in the CA extract. The sharp peak at 1021 corresponds to present of phosphate ion in the extract. The phenolic groups involved in ion replacement reactions are placed in the 1250–1270 cm^{-1} and 1485–1620 cm^{-1} spectrum of the plant extract. The peak at 1627 represents N–H bending in amide group and the peak at 2930 is accredited to asymmetric stretching of sp^3 carbon atoms. The broad peak found between 3280–3495 cm^{-1} is assigned to the stretching of the (–NH) aliphatic secondary groups present in the extract (Fig. 5).

3.7. UPLC-ESI MS/MS analysis of CA ethanolic seed extract

The UPLC-ESI-MS/MS analysis was performed for the identification of bioactive compounds of CA ethanolic seed extract. The bioactive compounds were identified based on molecular mass and retention time with database ResPect phytochemical software. The UPLC-ESI MS/MS analysis of both positive and negative ions modes was performed, and in total 40 compounds were identified. The detected compounds are listed in Table 4 along with their retention periods, molecular weights, molecular formula, and amounts (ppm). The robust antioxidative defense system of filarial parasites aids in evading the host oxidative attack mechanism. For the discovery of novel pharmaceuticals, molecular docking is a more expanding and cost effective alternative to the laborious *in vitro* drug screening procedure. The 25 most abundant CA bioactive compounds were selected for *in silico* screening against the forementioned filarial anti-oxidant proteins/enzymes. Based on binding energy values the 10 top scoring bioactive compounds namely 3-*O*-methyl-quercitin, 4-methoxycinnamoyloleanolic acid methyl ester, carbenicillin, podorhizol-β-D glucoside, RU5135, soraphen A, beta-obscurine, carbenicillin, vanillin, gentisic acid, and quinic acid were chosen for further *in silico* studies (Table 5 and Fig. 6).

3.8. Molecular docking of CA bioactive compounds

The drug-likeness properties of bioactive compounds were checked by the Lipinski filter and their Absorption, Distribution, Metabolism, Excretion, and Toxicity properties were analyzed by admetSAR server (Table 6). Out of the 10 bioactive compounds of CA, only five confirmed to be safe and non-toxic
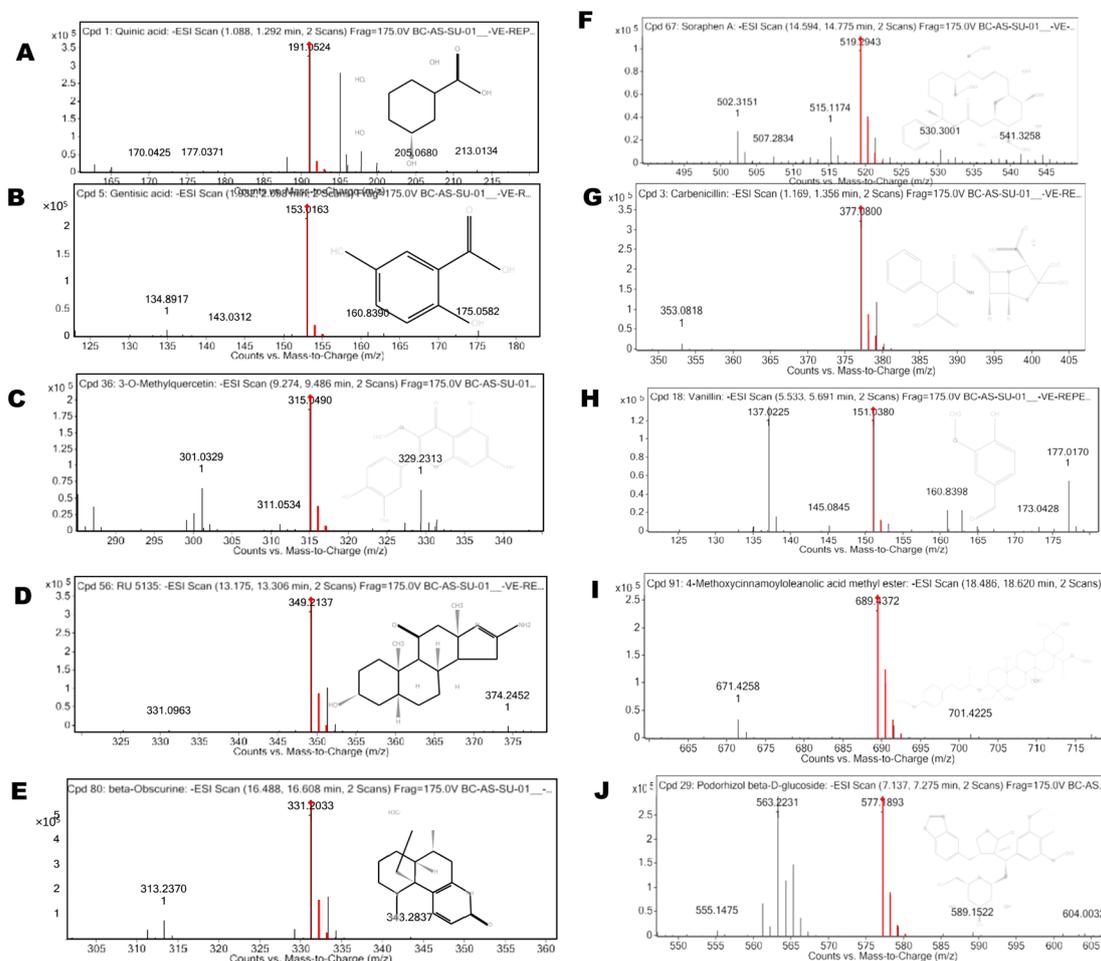

Fig. 6 Graphical representation of LC-MS/MS spectra and fragmentation profile of CA bioactive compounds.

Table 6 AdmetSAR properties of selected CA bioactive compound used in docking analysis

Parameter	3-O-methylquercetin	4-Methoxycinnamoyloleanolic acid methyl ester	Albendazole	DEC	Beta-obscurine	RU 5135	Soraphen A	Carbenicillin	Gentisic acid	Quinic acid	Vanillin	Podorhizol beta-D-glucoside
Blood brain barrier	BBB−	BBB+	BBB+	BBB+	BBB+	BBB+	BBB−	BBB−	BBB+	BBB+	BBB+	BBB−
Human intestinal absorption	HIA+	HIA−	HIA+	HIA+	HIA+	HIA+	HIA−	HIA−	HIA+	HIA+	HIA+	HIA−
Coco-2 permeability	Caco2+	Caco2+	Caco2−	Caco2+	Caco2+	Caco2−	Caco2+	Caco2−	Caco2+	Caco2−	Caco2+	Caco2−
P-glycoprotein substrate	Substrate	Substrate	No substrate	Substrate	Substrate	Substrate	Substrate	Substrate	No substrate	No substrate	No substrate	Substrate
hERG	Weak inhibitor	Weak inhibitor	Weak inhibitor	Weak inhibitor	Weak inhibitor	Weak inhibitor	Weak inhibitor	Weak inhibitor	Weak inhibitor	Weak inhibitor	Weak inhibitor	Weak inhibitor
AMES toxicity	Non AMES toxic	Non AMES toxic	Non AMES toxic	Non AMES toxic	Non AMES toxic	Non AMES toxic	Non AMES toxic	Non AMES toxic	Non AMES toxic	Non AMES toxic	Non AMES toxic	Non AMES toxic
Carcinogens	Non carcinogen	Non carcinogen	Non carcinogen	Non carcinogen	Non carcinogen	Non carcinogen	Non carcinogen	Non carcinogen	Non carcinogen	Non carcinogen	Non carcinogen	Non carcinogen
Acute oral toxicity	III	III	III	III	III	III	III	IV	III	III	III	III
Rat acute toxicity	2.6388 LD$_{50}$ mol kg^{-1}	2.0343 LD$_{50}$ mol kg^{-1}	2.0752 LD$_{50}$ mol kg^{-1}	2.2639 LD$_{50}$ mol kg^{-1}	2.9623 LD$_{50}$ mol kg^{-1}	2.6484 LD$_{50}$ mol kg^{-1}	3.0223 LD$_{50}$ mol kg^{-1}	1.4399 LD$_{50}$ mol kg^{-1}	2.1788 LD$_{50}$ mol kg^{-1}	1.7528 LD$_{50}$ mol kg^{-1}	1.9642 LD$_{50}$ mol kg^{-1}	2.6524 LD$_{50}$ mol kg^{-1}
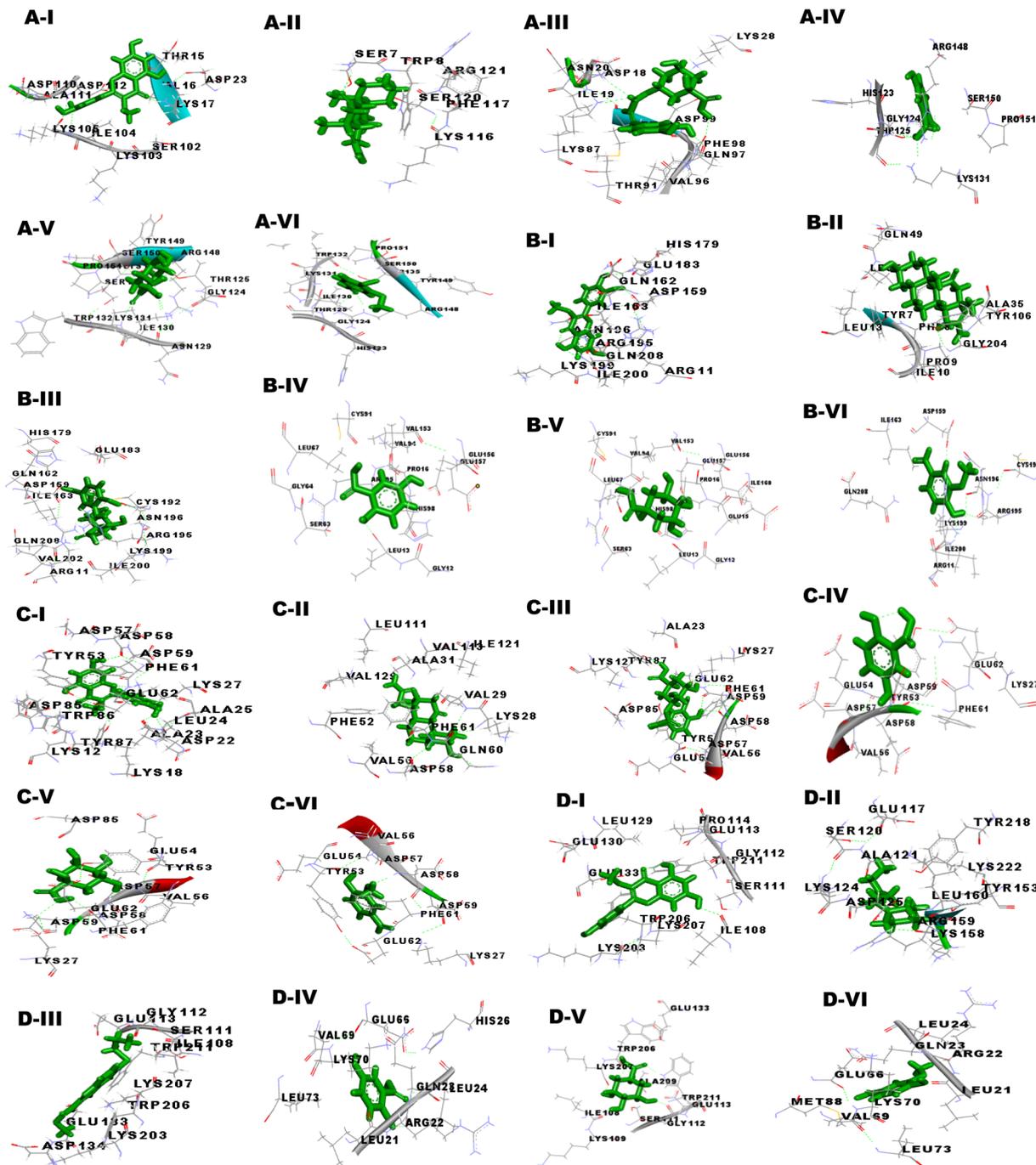
Fig. 7 Visualization of 3D interaction of filarial antioxidant enzyme/proteins with bioactive compounds of CA extract with anti-filarial drugs. The ligands were represented by a stick model in green color, whereas interacting residues were labeled in black color (A) glutathione peroxidase, (B) glutathione-S-transferase, (C) thioredoxin (D) superoxide dismutase, and (I) 3-O-methylquercetin, (II) DEC, (III) Albendazole, (IV) gentisic acid, (V) quinic acid, (VI) vanillin.

as predicted by the admetSAR values. The bioactive compounds 3-O-methylquercetin, vanillin, gentisic acid, and quinic acid only were used for further simulation studies. The 3D interactions of these CA bioactive compounds with the antioxidant proteins were visualized through BIOVIA Discovery Studio (Fig. 7).

Our studies targeted the antioxidant proteins *i.e.* glutathione-S-transferase (GST), thioredoxin (TRx), glutathione

Table 7 Docking summary of antioxidant proteins with bioactive compounds of CA binding energy, dissociation constant, from YASARA software, GSH score, and AI area from PatchDock server

Receptor	S. n.	Ligand	Binding energy (kcal mol^{-1})	Dissociation constant (μm)	Score	Area	ACE
Glutathione peroxidase	1	4-Methoxycinnamoyloleanolic acid methyl ester	7.540	2.967	5448	647.70	−174.14
	2	3-O-methylquercetin	6.026	8.272	3864	500.00	−243.56
	3	RU 5135	4.312	246.392	4576	555.70	−219.07
	4	Podorhizol beta-ᴅ-glucoside	6.443	18.932	5060	748.80	−430.03
	5	Vanillin	4.782	312.426	2945	372.1	−123.40
	6	Soraphen A	5.801	55.951	3764	401.6	−30.84
	7	Gentisic acid	5.944	23.684	3010	310.5	−125.61
	8	Quinic acid	5.427	105.1855	3066	322.4	−115.59
	9	Carbenicillin	5.443	112.013	3129	298.3	−124.41
	10	Albendazole	5.016	210.486	3698	397.90	−165.80
	11	DEC	4.189	850.006	3708	454.50	−212.10
	12	Beta-obscurine	4.012	910.020	3001	129.70	−80.01
Glutathione-S-transferase	1	4-Methoxycinnamoyloleanolic acid methyl ester	8.756	0.381	5830	848.9	−68.31
	2	3-O-methylquercetin	6.907	8.651	3746	450.5	−97.94
	3	RU 5135	4.109	135.196	3488	492.5	−192.03
	4	Vanillin	4.757	325.891	3134	355.69	−105.40
	5	Podorhizol beta-ᴅ-glucoside	7.309	4.389	4802	599.3	−138.33
	6	Soraphen A	6.472	18.028	3730	486	−109.89
	7	Carbenicillin	6.243	32.013	3629	298.3	−64.41
	8	Gentisic acid	6.019	11.727	2706	305.3	−86.24
	9	Quinic acid	5.869	49.884	2790	327.7	−84.51
	10	Albendazole	5.025	207.312	3540	466.6	−140.15
	11	DEC	4.215	13.512	3314	414.1	−151.11
	12	Beta-obscurine	3.929	928.020	3101	239.70	−94.21
Thioredoxin transferase	1	4-Methoxycinnamoyloleanolic acid methyl ester	7.786	1.962	5324	587.3	2.92
	2	3-O-methylquercetin	6.727	7.723	3920	423.6	−177.16
	3	RU 5135	3.987	113.250	3432	377.5	−45.57
	4	Beta-obscurine	4.204	112.187	2994	331.7	−50.98
	5	Soraphen A	6.728	11.703	3520	383.7	−117.43
	6	Carbenicillin	6.518	16.681	3992	454.3	−163.83
	7	Vanillin	4.975	225.567	3092	394.1	−91.2
	8	Gentisic acid	5.605	7.889	4290	493.8	−8.56
	9	Quinic acid	5.379	114.061	2208	277	−80.32
	10	Albendazole	5.250	141.807	3374	363.3	−98.38
	11	DEC	4.521	485.358	3000	320.2	−95.42
	12	Podorhizol beta-ᴅ-glucoside	7.491	4.389	4792	569.3	−128.33
Superoxide dismutase	1	4-Methoxycinnamoyloleanolic acid methyl ester	8.420	0.6730	5480	629.9	−50.26
	2	3-O-methylquercetin	6.177	9.661	3352	415.4	−111.54
	3	RU 5135	4.035	111.565	3154	361.9	−100.79
	4	Beta-obscurine	3.595	114.648	2968	320.6	29.8
	5	Carbenicillin	6.048	36.877	3934	475.5	−212.64
	6	Vanillin	4.503	500.330	2948	226.1	−21.4
	7	Soraphen A	5.728	91.703	3520	383.7	−57.43
	8	Gentisic acid	4.967	8.633	2282	252.3	6.44
	9	Quinic acid	5.726	63.501	2316	255.9	27.02
	10	Albendazole	5.358	118.177	3648	413.9	−109.75
	11	DEC	4.252	764.262	2936	342.3	−4.55
	12	Podorhizol beta-ᴅ-glucoside	7.191	6.389	4692	499.3	−138.33

peroxidase (GPx), and superoxide dismutase (SOD). The GPx model was validated by the RAMPAGE server, as well as the PDBsum and ProCheck servers showed that none of the amino acids were located in the disallowed region. Further, the quality of the 3D model was examined by ERRAT, ProSA and RAMPAGE servers. Metapocket 2.0 server was used to predict the binding site of GPx and the top 3 binding sites were considered as the active sites of protein (S Table 1†). The PatchDock server and YASARA tool were used to investigate the docking characteristics of CA bioactive compounds with filarial antioxidant proteins. The following parameters were studied in this work: (a) interacting amino acid residue, (b) interacting residue active site number, (c) CA bioactive compounds and antioxidant proteins involved in the H-bonding, (d) binding energy, (e)

dissociation constant, (f) GSC score, and (g) AI area. Interacting residues were identified using the YASARA programme and the PatchDock server, and notable binding sites were predicted with the Metapocket 2.0 server and Discovery Studio 3.5. The retrieved docked complexes were screened for the highest binding energy, lowest dissociation constant, maximum hydrogen bonding, higher GSC score, AI area, and docking within the top three binding sites of anti-oxidant proteins, GST, GPx, SOD, and TRx, with only the best complex being chosen for further analysis. On the basis of docking studies CA bioactive compounds 4-methoxycinnamoyloleanolic acid methyl ester, 3-*O*-methylquercetin, Podorhizol β D-glucoside, and soraphen A had the highest computed binding energies. The binding energies of these compounds were much higher than anti-filarial drugs Albendazole and DEC (Table 7). The docking analysis also showed that CA bioactive compounds and anti-oxidant proteins could form ample hydrogen bonds with one another. Soraphen A, 3-*O*-methylquercetin and quinic acid showed maximum hydrogen bonding among all CA bioactive compounds, forming 8, 7 and 5 bonds with GST, TRx and GR respectively. Also, the interacting amino acid residues were mostly found in the predicted binding sites of the antioxidant proteins.

3.9. Molecular dynamics simulation analysis

The MD run took place in an isothermal, isobaric (NPT) ensemble (310 K and 1 bar) for 50 nanoseconds (ns). Due to their stronger interactions and comparatively higher binding energies in molecular docking, we chose 3-*O*-methylquercetin, quinic acid, gentisic acid, and vanillin for the MD run. For each target, the MD simulations of individual filarial GST, TRx, SOD, and GR with water were used as control.

The Root Mean Square Deviation (RMSD) of the protein ligand complexes of filarial antioxidant proteins and CA bioactive compounds is shown in Fig. 8. In the entire, MD simulation run, RMSD of GST ranged from 1.316 Å to 2.022 Å and was lowest with gentisic acid. The RMSD for TRx's inter-action with 3-*O*-methylquercetin was in the range of 2.03–4.743 Å whereas for SOD it was 4.39–10.75 Å. The anti-oxidant protein GPx formed most stable complexes with all CA bioac-tive compounds and the variation in RMSD was less than 1 Å
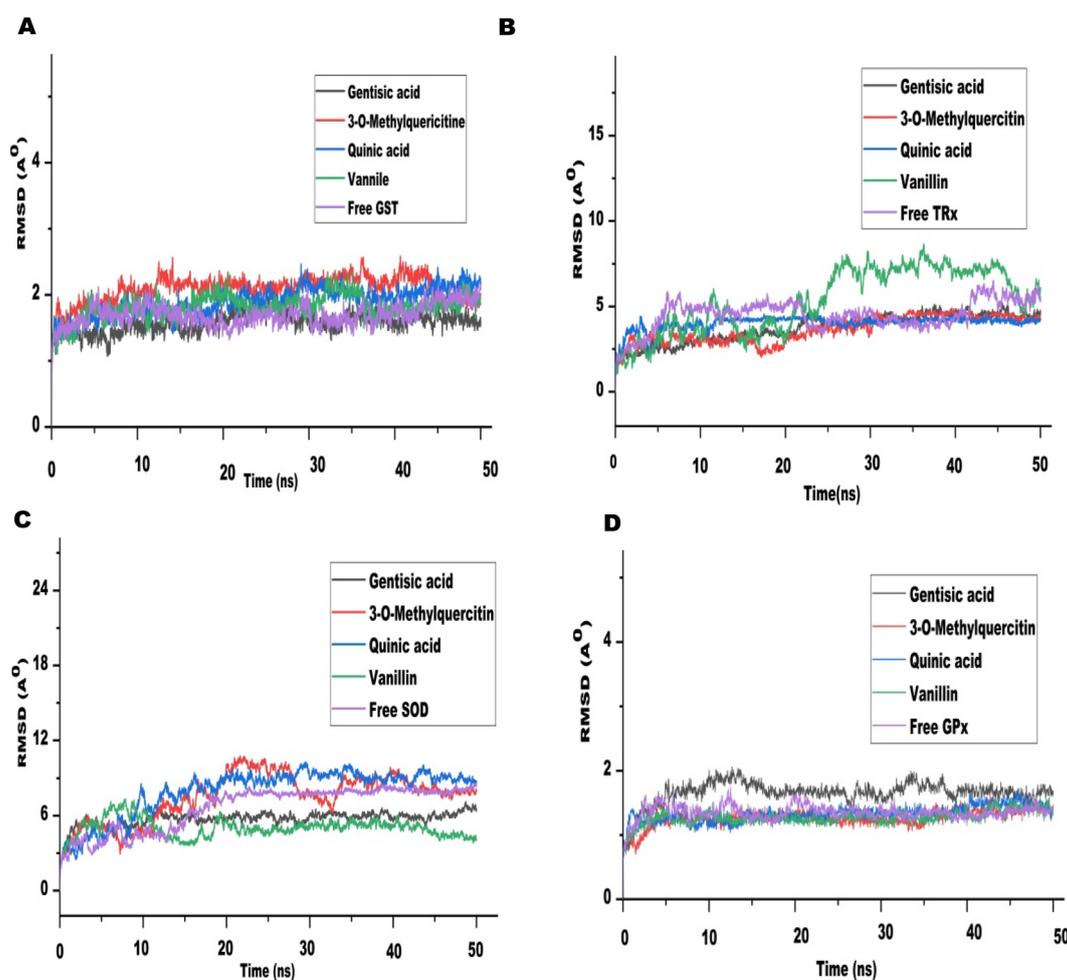

Fig. 8 The RMSD of filarial antioxidant proteins/enzymes complexed with CA bioactive compounds as a function of 50 ns. (A) RMSD of complexed and free GST. (B) RMSD of Cα-atoms of complexed and free TRx. (C) RMSD of Cα-atoms of complexed and free SOD. (D) RMSD of Cα-atoms of complexed and free GPx.
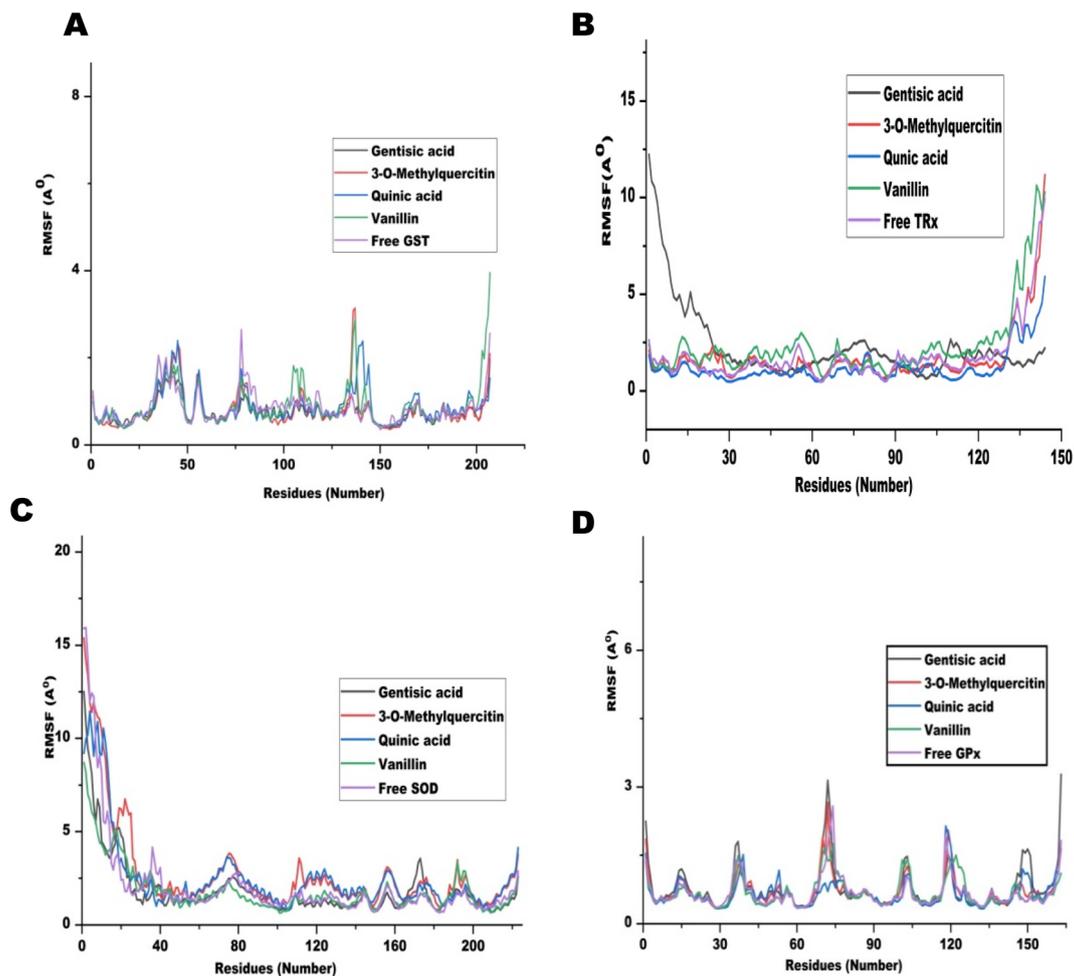
Fig. 9 The RMSF of filarial antioxidant proteins/enzymes with CA bioactive compounds as a function of 50 ns. (A) RMSF analysis of amino acid residues of complexed and free GST. (B) RMSF analysis of amino acid residues of complexed and free TRX. (C) RMSF analysis of amino acid residues of complexed and free SOD. (D) RMSF analysis of amino acid residues of complexed and free GPx.

with 3-*O*-methylquercetine. Upon comparison of average RMSD values for protein-ligand complexes, 3-*O*-methylquercetin and gentisic acid formed most stable complexes with filarial antioxidant proteins. During the entire run, the total energy, potential energy, and temperature remained constant and the RMSD of each docked complex was below 10 Å.[46] The interaction between the ligand and protein residue was demonstrated by the Root Mean Square Fluctuation (RMSF).[11] The graph of antioxidant proteins with CA bioactive compounds is represented in Fig. 9. The attachment stability of binding with the amino acids sequence over a given time period, such as the ligand, can be established using RMSF analysis. In comparison to other locations fluctuation were more frequent at the N- and C-terminal regions in all the complexes. The RMSF graph of GST showed minor deviations in amino acid residues at positions 136 to 144 during the

simulation run. The RMSF of TRx complex with CA bioactive compounds shows fluctuation between 132 to 144 amino acid residues. The RMSF of SOD complexes initially fluctuated between 1 to 20 amino acid residues, but later less pronounced oscillations were seen throughout the complete run. The minor fluctuations of GPx complex with CA bioactive compounds was observed in between 69 to 76 amino acid residues. The compactness of CA bioactive compounds was analyzed by radius of gyration (R_g) plots and depicted in Fig. 10. The average radius of gyration of GPx with 3-*O*-methylquercetin was least (18.359) among all the bioactive compounds. Quinic acid complexes with GST and TRx had most stable complex structure with an average radius of gyration values of 21.080 Å and 19.085 Å respectively. Furthermore SOD complex with vanillin had the lowest R_g value of 26.95 Å.
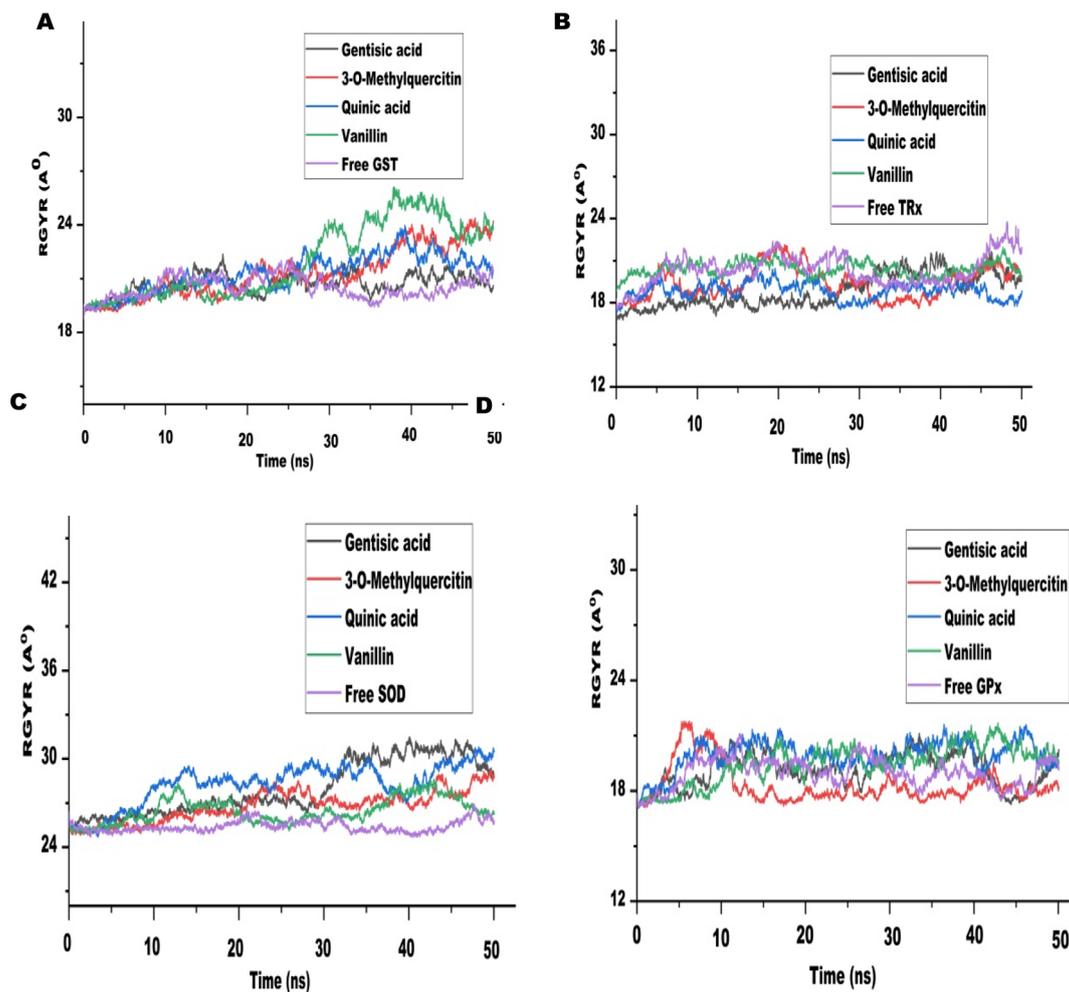
Fig. 10 The radius of gyration (R_g) of filarial antioxidant proteins/enzymes with CA bioactive compounds as a function of time 50 ns. (A) R_g of complexed and free GST. (B) R_g of complex and free TRx. (C) R_g of complex and free SOD. (D) R_g of complex and free GPx.

4 Conclusion

In the present work, CA seed extract was prepared using a sustainable, efficient, and easily reproducible approach. The seed extract from CA significantly increased the levels of ROS, antioxidant proteins/enzymes, thus disrupting the redox balance of the filarial parasites. Overall, the CA treatment had a huge impact on the metabolism and survival of *S. cervi* filarial parasites, demonstrating excellent efficacy even at extremely low doses. Further the HRAMS proteomics results demonstrated that the parasites' exposures to CA extract led to the disruption of crucial signaling and metabolic pathways. The bioactive components in CA such as sterols, tannin, terpenes, fatty acids, lactones, phenolics, tetrahydroxyflavone, flavonoids, cyclic polyol, and benzoic acid are known to have several biological activities. The *in silico* studies proved that CA bioactive compounds like 3-*O*-methylquercetin, quinic acid, vanillin, and gentisic acid could stably interact with the parasites anti-oxidant proteins GPx, TRx, SOD, and GST. Hence, on the basis of biochemical, HRAMS, molecular docking, and *in silico* simulation studies, it seems imperative to integrate CA as a future treatment modality for Lymphatic Filariasis.

Ethical statement

Data availability

All data supporting the finding of this study are available within the paper and its ESI.†

Author contributions

Sunil Kumar: conceptualization, methodology, data curation, formal analysis, investigation, writing – original draft, review & editing. Ayushi Mishra: methodology, formal analysis, investigation, review & editing. Surya Pratap Singh: review & editing.

Conflicts of interest

The authors declare no conflict of interest.

Acknowledgements

References

1 D. J. Tisch, E. Michael and J. W. Kazura, *Lancet Infect. Dis.*, 2005, **5**, 514–523.

2 R. K. Prichard, M.-G. Basanez, B. A. Boatin, J. S. McCarthy, H. H. Garcia, G.-J. Yang, B. Sripa and S. Lustigman, *PLoS Neglected Trop. Dis.*, 2012, **6**, e1549.

3 J. N. Sangshetti, D. B. Shinde, A. Kulkarni and R. Arote, *RSC Adv.*, 2017, **7**, 20628–20666.

4 O. Ojurongbe, A. A. Akindele, M. A. Adeleke, M. O. Oyedeji, S. A. Adedokun, J. F. Ojo, C. A. Akinleye, O. S. Bolaji, O. A. Adefioye and O. A. Adeyeba, *PLoS Neglected Trop. Dis.*, 2015, **9**, e0003633.

5 R. Prichard, *Human and Animal Filariases: Landscape, Challenges, and Control*, 2022, pp. 283–305.

6 A. Singh, A. Mishra, R. Chaudhary and V. Kumar, *J. Sci. Res.*, 2020, **64**, 50–58.

7 C. Y. Looi, B. Moharram, M. Paydar, Y. L. Wong, K. H. Leong, K. Mohamad, A. Arya, W. F. Wong and M. R. Mustafa, *BMC Complementary Altern. Med.*, 2013, **13**, 1–14.

8 S. Sharma and B. Mehta, *J. Hyg., Epidemiol., Microbiol., Immunol.*, 1991, **35**, 157–161.

9 A. Arya, C. Y. Looi, S. C. Cheah, M. R. Mustafa and M. A. Mohd, *J. Ethnopharmacol.*, 2012, **144**, 22–32.

10 K. Singhal, S. Sharma and B. Mehta, *Indian J. Exp. Biol.*, 1992, **30**, 546–548.

11 V. Kumar, A. Mishra and A. Singh, *RSC Adv.*, 2022, **12**, 22542–22554.

12 A. Singh and S. Rathaur, *Biochem. Biophys. Res. Commun.*, 2005, **331**, 1069–1074.

13 S. Sharma, F. Ahmad, A. Singh and S. Rathaur, *Vet. Parasitol.*, 2021, **290**, 109357.

14 S. Yadav, S. Sharma, F. Ahmad and S. Rathaur, *J. Drug Delivery Sci. Technol.*, 2020, **56**, 101557.

15 T. Mosmann and T. Fong, *J. Immunol. Methods*, 1989, **116**, 151–158.

16 H. Sim Choi, J. Woo Kim, Y. N. Cha and C. Kim, *J. Immunoassay Immunochem.*, 2006, **27**, 31–44.

17 A. Nayak, P. Gayen, P. Saini, N. Mukherjee and S. P. Sinha Babu, *Parasitol. Res.*, 2012, **111**, 1173–1186.

18 W. M. Nauseef and R. A. Clark, *NADPH Oxidases: Methods and Protocols*, 2019, pp. 3–16.

19 E. Shacter, J. A. Williams, M. Lim and R. L. Levine, *Free Radicals Biol. Med.*, 1994, **17**, 429–437.

20 B. Halliwell and S. Chirico, *Am. J. Clin. Nutr.*, 1993, **57**(5), 715S–724S.

21 S. Rathaur, M. Yadav, N. Singh and A. Singh, *J. Proteomics*, 2011, **74**, 1595–1606.

22 S. Tiwari, M. Wadhawan, N. Singh and S. Rathaur, *J. Proteomics*, 2015, **113**, 435–446.

23 M. Wadhawan, F. Ahmad, S. Yadav and S. Rathaur, *Protein J.*, 2022, **41**, 613–624.

24 V. Kumar, A. Mishra, A. K. Yadav, S. Rathaur and A. Singh, *Plos One*, 2022, **17**(7), e0270635.

25 A. Mishra, S. Kumar and A. Singh, *RSC Adv.*, 2024, **14**, 5893–5906.

26 H. Birla, C. Keswani, S. S. Singh, W. Zahra, H. Dilnashin, A. S. Rathore, R. Singh, M. Rajput, P. Keshri and S. P. Singh, *ACS Chem. Neurosci.*, 2021, **12**, 4319–4335.

27 A. Mishra, V. Kumar and A. Singh, *Pharm. Biol.*, 2022, **60**, 2237–2252.

28 L. Willard, A. Ranjan, H. Zhang, H. Monzavi, R. F. Boyko, B. D. Sykes and D. S. Wishart, *Nucleic Acids Res.*, 2003, **31**, 3316–3319.

29 B. Huang, *OMICS: J. Integr. Biol.*, 2009, **13**, 325–330.

30 F. Amir and K. Y. Chin, *Int. J. PharmTech Res.*, 2011, **3**, 1772–1779.

31 A. B. D. Nandiyanto, R. Oktiani and R. Ragadhita, *Indones. J. Sci. Technol.*, 2019, **4**, 97–118.

32 Y. Sawada, R. Nakabayashi, Y. Yamada, M. Suzuki, M. Sato, A. Sakata, K. Akiyama, T. Sakurai, F. Matsuda and T. Aoki, *Phytochemistry*, 2012, **82**, 38–45.

33 S. Kim, J. Chen, T. Cheng, A. Gindulyte, J. He, S. He, Q. Li, B. A. Shoemaker, P. A. Thiessen and B. Yu, *Nucleic Acids Res.*, 2021, **49**, D1388–D1395.

34 C. Lipinski and A. Hopkins, *Nature*, 2004, **432**, 855–861.

35 F. Cheng, W. Li, Y. Zhou, J. Shen, Z. Wu, G. Liu, P. W. Lee and Y. Tang, *J. Chem. Inf. Model.*, 2012, **52**(11), 3099–3105.

36 D. Schneidman-Duhovny, Y. Inbar, R. Nussinov and H. J. Wolfson, *Nucleic Acids Res.*, 2005, **33**, W363–W367.

37 E. Krieger and G. Vriend, *Bioinformatics*, 2014, **30**, 2981–2982.

38 C. Y. Looi, A. Arya, F. K. Cheah, B. Muharram, K. H. Leong, K. Mohamad, W. F. Wong, N. Rai and M. R. Mustafa, *PLoS One*, 2013, **8**, e56643.

39 H. C. Santiago, S. Bennuru, A. Boyd, M. Eberhard and T. B. Nutman, *J. Allergy Clin. Immunol.*, 2011, **127**, 479–486.

40 J. Magalhães, J. Eira and M. A. Liz, *Cell. Mol. Life Sci.*, 2021, **78**, 6105–6117.

41 L. Beld, H. Jung, C. A. Bulman, B. A. Rosa, P. U. Fischer, J. W. Janetka, S. Lustigman, J. A. Sakanari and M. Mitreva, *Pathogens*, 2022, **11**, 707.

42 P. M. Cromm and C. M. Crews, *ACS Cent. Sci.*, 2017, **3**, 830–838.

43 B. Dahlmann, *BMC Biochem.*, 2007, **8**, 1–12.

44 M. D. Bartolowits, J. M. Gast, A. J. Hasler, A. M. Cirrincione, R. J. O'Connor, A. H. Mahmoud, M. A. Lill and V. J. Davisson, *ACS Omega*, 2019, **4**, 15181–15196.

45 S. O. Wendel, J. A. Snow, L. Gu, N. S. Banerjee, L. Malkas and N. A. Wallace, *J. Med. Virol.*, 2023, **95**, e29244.

46 C. B. M. Platania and C. Bucolo, *Allostery: Methods and Protocols*, 2021, pp. 245–254.